HHS Public Access

Author manuscript

Dev Biol. Author manuscript; available in PMC 2018 April 26.

Published in final edited form as:

Dev Biol. 2008 September 15; 321(2): 500–514. doi:10.1016/j.ydbio.2008.04.005.

Pbx1/Pbx2 govern axial skeletal development by controlling Polycomb and *Hox* in mesoderm and *Pax1/Pax9* in sclerotome

Terence D. Capellini[1], **Rediet Zewdu**[*,1], **Giuseppina Di Giacomo**[*,1], **Stefania Asciutti**[1], **Jamie E. Kugler**[1], **Anna Di Gregorio**[1], and **Licia Selleri**[1,#]

[1]Department of Cell and Developmental Biology, Weill Medical College of Cornell University, 1300 York Avenue, New York, NY 10021, USA

Abstract

The post-cranial axial skeleton consists of a metameric series of vertebral bodies and intervertebral discs, as well as adjoining ribs and sternum. Patterning of individual vertebrae and distinct regions of the vertebral column is accomplished by Polycomb and Hox proteins in the paraxial mesoderm, while their subsequent morphogenesis depends partially on Pax1/Pax9 in the sclerotome. In this study, we uncover that *Pbx1/Pbx2* are co-expressed during successive stages of vertebral and rib development. Next, by exploiting a *Pbx1/Pbx2* loss-of-function mouse, we show that decreasing *Pbx2* dosage in the absence of *Pbx1* affects axial development more severely than single loss of *Pbx1*. *Pbx1/Pbx2* mutants exhibit a homogeneous vertebral column, with loss of vertebral identity, rudimentary ribs, and rostral hindlimb shifts. Of note, these axial defects do not arise from perturbed notochord function, as cellular proliferation, apoptosis, and expression of regulators of notochord signaling are normal in *Pbx1/Pbx2* mutants. While the observed defects are consistent with loss of Pbx activity as a Hox-cofactor in the mesoderm, we additionally establish that axial skeletal patterning and hindlimb positioning are governed by *Pbx1/Pbx2* through their genetic control of Polycomb and *Hox* expression and spatial distribution in the mesoderm, as well as of *Pax1/Pax9* in the sclerotome.

Graphical abstract

[#]Corresponding author. lis2008@med.cornell.edu, Phone: 1-212-746-5009, Fax: 1-212-746-5596.
[*]These authors contributed equally to this work.

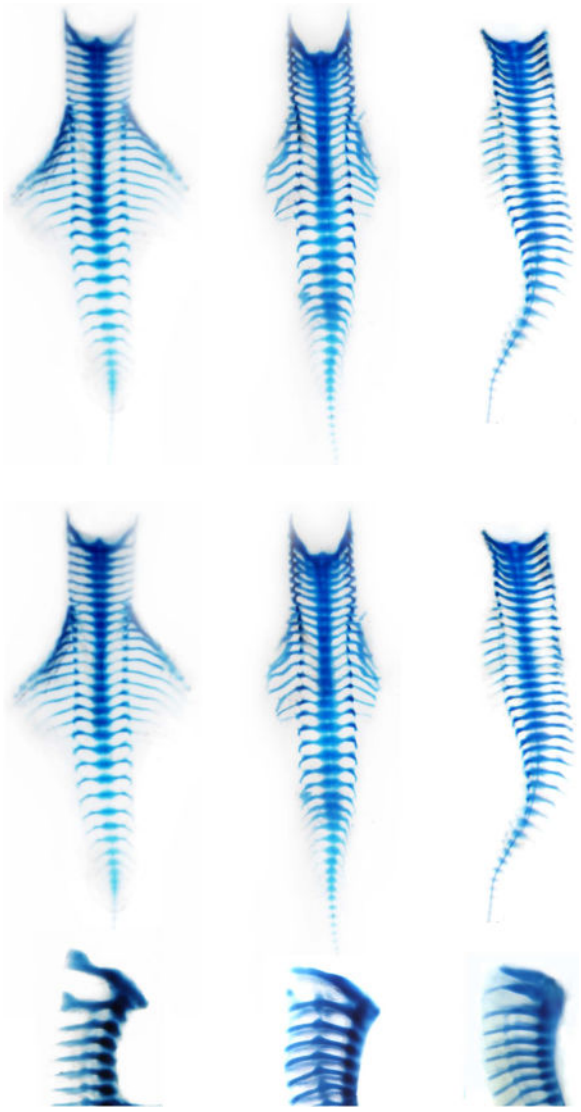

Keywords

Axial skeleton; Hox; limb position; Meis/Prep; notochord; Pax; Pbx; Polycomb; sclerotome; vertebrae

Introduction

The vertebrate post-cranial axial skeleton consists of a metameric series of elements comprising the vertebral bodies, intervertebral discs, and proximal ribs (primaxial component), as well as the sternum and sternal ribs (abaxial component)(Christ and Wilting, 1992, Liem et al., 2001; Nowicki and Burke, 2000). The primaxial pattern, consisting of distinct cervical, thoracic, lumbar, sacral, and caudal vertebrae as well as proximal ribs, is initially laid down during somite formation and differentiation, whereas the abaxial pattern derives from the lateral plate mesoderm (LPM). During somite formation blocks of paraxial

mesodermal (PM) cells on both sides of the neural tube arise from undifferentiated pre-somitic mesoderm, while in somite differentiation a ventral compartment of this mesoderm forms the mesenchymal sclerotome (Christ et al., 2004). At the onset of vertebral formation, ventro-medial sclerotomal cells migrate medially, condense into a uniform density, and form a segmented pattern that gives rise to the distinct vertebral bodies and the annuli fibrosi of the intervertebral discs. Likewise, lateral sclerotomal cells migrate, but do so dorsally to form the vertebral pedicles and the laminae of the neural arches as well as the proximal portions of ribs (Christ and Wilting, 1992).

Both somite formation and differentiation are dependent upon molecular signals from the notochord (Cleaver and Krieg, 2001; Liem et al., 2000; Pourquie et al., 1993; Stemple, 2005; Watterson et al., 1954). Indeed, the availability of mouse notochord mutants, such as *undulated* (*un*; Balling et al., 1988; Chalepakis et al., 1991; Dietrich and Gruss, 1995; Wallin et al., 1994) and *Danforth short tail* (*Sd*; Koseki et al., 1993), which display specific malformations in vertebral column development, has led to the firm conclusion that notochord signaling to the somites is required for proper formation of the cartilaginous axial skeleton. In vertebrates, the notochord is eventually replaced by the vertebral column, and its remnants form the *nuclei pulposi* of the intervertebral discs (Hunter et al., 2004; Smits and Lefebvre, 2003).

Numerous genes have been shown to play roles in post-cranial axial skeletal development and, in this regard, Hox transcription factors were among the first discovered (Kmita and Duboule, 2003; Krumlauf, 1994; Wellik, 2007). While it has been demonstrated in zebrafish that four *Hox* genes (*hoxb1, hoxb5, hoxc6*, and *hoxc8*) are expressed within the developing notochord where they may function in patterning (Prince et al., 1998), *Hox* expression and function in the mammalian notochord has not been extensively analyzed. Most research on *Hox* indicates that their patterning roles take place in the developing PM and LPM during axial differentiation where they establish rostral-caudal expression boundaries that lead to the regionalization of the vertebral metameric pattern and to the establishment of the distinctive characteristics of vertebrae and ribs (reviewed in Favier and Dolle, 1997; and Wellik, 2007; Nowicki and Burke, 2000; Wellik and Capecchi, 2003). For example, compound mutants for specific *Hox* paralogs, such as *Hox5, Hox6*, and *Hox9*, exhibit drastic transformations in the thoracic region, including rib and sternal defects (McIntyre et al., 2007). Importantly, these global aspects of *Hox*-based axial skeletal patterning are not apparent in mice that are mutant for only single paralogous alleles, due to the high redundancy among the different paralogous family members (Wellik, 2007).

Hox-based patterning of the vertebral column partially depends on the action of Polycomb group genes, whose function is to repress *Hox* gene transcription in somites rostral to *Hox* expression domains and to aid in the maintenance of the boundary conditions that help specify the distinctively patterned vertebrae (Kim et al., 2006). Recently, mutations for the mouse Polycomb genes, *Bmi* and *Eed*, have demonstrated that in both their individual and compound absence, *Hox* gene expression is shifted rostrally and vertebral identities are homeotically transformed and shifted across several regions of the vertebral column (Faust et al., 1995; 1998; Kim et al., 2006; Lessard et al., 1999; van der Lugt et al., 1994).

Later in mouse gestation, members of the Pax family of transcription factors (Robson et al., 2006) are also functionally required to regulate axial skeletal development. Among these, *Pax1* is active in the sclerotome (Deutsch et al., 1988), and the severity of the *Pax1* mutant phenotype in mice with different *Pax1* mutations indicates that its actions may be strongest in the lumbar region and the tail (Koseki et al., 1993). Indeed, *Pax1* mouse mutants, such as *un*, exhibit highly dysmorphic vertebral columns with lack of (or split) vertebral bodies, absence of intervertebral disks, and missing or severely malformed proximal ribs (Wallin et al., 1994). Interestingly, the severity of the *Pax1* vertebral phenotype is exacerbated when *Pax9* is concurrently lost (Peters *et al.*, 1999) due, at least in part, to altered control of *Bapx1* expression in the sclerotome (Rodrigo *et al.*, 2003). The finding that both *Pax* and *Hox* mutants have defects in similar skeletal structures suggests that they likely synergistically pattern structures of the axial skeleton (Aubin *et al.*, 2002).

Recently, critical roles of *Pbx* genes (*Pbx1–3*), which encode the TALE class of homeodomain-containing transcription factors (Burglin, 1997; 1998; Mukherjee and Bürglin, 2007), have been established in skeletal development (Capellini et al., 2006; Selleri et al., 2001). During the past decade, Pbx TALE homeodomain proteins have been mainly regarded as Hox cofactors, i.e. ancillary factors that increase Hox DNA-binding specificity and selectivity (reviewed by Mann and Affolter, 1998; Mann and Chan, 1996; Moens and Selleri, 2006). It has further been demonstrated that Pbx proteins, when forming complexes with Hox proteins (and with other partner proteins of the Meis family), lead to the transcriptional regulation of *Hox* genes themselves as well as other target genes (Capellini et al., 2006; Ferretti et al., 2000; Jacobs et al., 1999; Maconochie et al., 1997; Popperl et al., 1995). However, more recent findings also suggest that Pbx proteins can function more broadly in a Hox-independent manner (Berkes et al., 2004; Knoepfler et al., 1999), as well as act as hierarchical regulators of 5' *Hox* genes (Capellini et al., 2006). Previously, it was demonstrated that *Pbx1* is required for proper patterning of both the axial and limb skeleton (Selleri et al., 2001). Conversely, it was found that absence of either *Pbx2* or *Pbx3* does not determine skeletal phenotypes (Rhee et al., 2004; Selleri et al., 2004). However, by exploiting a *Pbx1/Pbx2* loss-of-function mouse model, it was established that decreasing *Pbx2* dosage in the absence of *Pbx1* affects limb development more severely than the loss of *Pbx1* alone, with the appearance of novel distal limb abnormalities (Capellini et al., 2006). These data indicate that Pbx have overlapping functions during skeletal development.

In this study, it is first uncovered that *Pbx1/Pbx2*, as well as *Meis1/Meis2*, are highly expressed in the notochord and in the sclerotome and vertebral anlagen, unlike *Pbx3* and *Meis3*, which exhibit negligible expression in all of these tissues. Next, by exploiting a *Pbx1/Pbx2* loss-of-function mouse model, it is shown that despite the lack of axial skeletal abnormalities in $Pbx2^{-/-}$ embryos (Selleri et al., 2004) decreasing *Pbx2* dosage in the absence of *Pbx1* affects axial skeletal development more severely than the loss of *Pbx1* alone (Selleri et al., 2001). In fact, compound *Pbx1/Pbx2* mutant embryos exhibit a homogeneous vertebral column morphology characterized by the marked flattening of all vertebral bodies, the thinning of the laminae, the loss of identity of the transverse processes in all regions of the vertebral column, as well as the presence of rudimentary ribs. Additionally, compound *Pbx1/Pbx2* mutant embryos display shifts in hindlimb positioning, which are concurrent with the alterations in vertebral identity and morphogenesis. Of note,

all of these defects do not appear to arise from perturbed notochord function, as morphology, cellular proliferation, and apoptosis, as well as expression of critical regulators of notochord signaling are normal in *Pbx1/Pbx2* mutants. While the observed defects are consistent with loss of Pbx activity as a Hox-cofactor in the mesoderm, we additionally establish that axial skeletal patterning and hindlimb positioning are governed by *Pbx1/Pbx2* through their genetic control of Polycomb and *Hox* expression and spatial distribution in the mesoderm, as well as of *Pax1/Pax9* in the sclerotome.

Materials and Methods

Mice

Intercrosses of $Pbx1^{+/-}$(Selleri et al., 2001) and $Pbx2^{+/-}$ (Selleri et al., 2004) were carried out in order to obtain $Pbx1^{+/-}Pbx2^{+/-}$ double heterozygotes. On a C57BL/6 background the number of double heterozygotes obtained was well below the expected Mendelian ratio. To increase their number, C57BL/6 double heterozygous males were crossed to an outbred strain, Black Swiss [NIH-BL(S)]. Next, double heterozygous C57BL/6 females and mixed double heterozygous C57BL/6-Black Swiss males were intercrossed and their progeny was analyzed for lethality as well as soft and hard tissue morphologies. In subsequent generations on mixed genetic backgrounds, a significant amelioration of the C57BL/6 limb but not axial skeletal phenotype was observed.

Histology and immunohistochemistry

For histological analysis, embryos were fixed in formalin and embedded in paraffin for sectioning using standard procedures. 5 μm sections were stained with Hematoxylin and Eosin, mounted in DPX, and photographed using a Magnafire digital camera (Optronix). Immunohistochemistry was performed on somite-matched mouse embryos at different gestational days, fixed with 4% paraformaldehyde (PFA) in phosphate-buffered saline (PBS) overnight (O/N) and processed for immunohistochemistry (Capellini et al., 2006). Paraffin sections were dewaxed and then treated by a microwave antigen retrieval step. The primary antibodies used to detect Pbx1, Pbx2, Pbx3, Meis, and Prep1 proteins were: a Pbx1b-specific monoclonal antibody (αPbx1b; Jacobs et al., 1999); a Pbx2-specific monoclonal antibody (G-20 sc-890; Santa Cruz); a Pbx3-specific monoclonal antibody (αPbx3a; Rhee et al., 2004); a Pan Meis-specific monoclonal antibody (αMeis; Jacobs et al., 1999) and a Prep1-specific monoclonal antibody (αMeis4; Upstate USA, Inc., Lake Placid, NY). To detect the presence of Phospho Histone H3, an antibody for Rabbit polyclonal Anti-phospho histone H3 (Ser10; Upstate USA) was utilized (Hendzel et al., 1997). To detect neurofilament staining on whole embryos at E11.5 and E12.5, an anti-2H3 neurofilament monoclonal antibody was acquired (as developed by T. Jessell and J. Dodd, and obtained from the Developmental Studies Hybridoma Bank, under the auspices of the NICHD, maintained by The University of Iowa, Department of Biological Sciences, Iowa City, IA 52242) and whole-mount immunohistochemistry was performed according to the protocols described in Capellini et al. (2006).

Skeletal preparations

Differential staining of cartilage and bone in mouse embryos (E13.5) was visualized using Alcian Blue and Alizarin Red (Selleri et al., 2001). Individual vertebral skeletal elements were dissected, isolated, and photographed (as described above) in glycerol in an agarose plate to ensure proper and consistent orientation.

Whole-mount *in situ* hybridization

Whole-mount *in situ* hybridizations were performed on somite-matched embryos at different gestational days using digoxygenin-labeled antisense RNA probes as previously described (Di Giacomo et al., 2006; Selleri et al., 2001). Probes for *Bmi* (Kim et al., 2006), *Col2a1* (Cheah et al., 1991), *Eed* (Kim et al., 2006), *Hoxa4* (Toth et al., 1987), *Hoxb5* (Krumlauf et al., 1987), *Hoxb8* (Charite et al., 1994), *Hoxc6* (Sharpe et al., 1988), *Hoxd3* (Condie and Capecchi, 1993), *Hoxd9* (Dolle et al., 1989), *Noggin* (Valenzuela et al., 1995), *Pax1* (Chalepakis et al., 1991), *Pax9* (Neubuser et al., 1995), and *Sox9* (Wright et al., 1995) were used.

Section *in situ* hybridization

Somite-matched embryos from E10.5 to E13 were harvested and fixed O/N at 4°C in PBS containing 4% PFA. Single-stranded sense and antisense riboprobes for *in situ* hybridization on frozen sections were synthesized for *Bapx1* (Tribioli et al., 1997), *Brachyury* (Wilkinson et al., 1990), *Col2a1* (Cheah et al., 1991), *Hoxb1* (Frohman et al., 1990), *Hoxb2* (Hunt et al., 1991), *Hoxc6* (Sharpe et al., 1988), *Hoxd9* (Dolle et al., 1989), *Meis1–3* (Capdevila et al., 1999), *Noggin* (Valenzuela et al., 1995), *Pax1* (Chalepakis et al., 1991), *Pbx1* (Brendolan et al., 2005), *Pbx2* (Selleri et al., 2004), *Pbx3* (Di Giacomo et al., 2006), *Shh* (Echelard et al., 1993) and *Sox9* (Wright et al., 1995).

Analysis of cellular proliferation

BrdU incorporation and cell density counting—Pregnant mice were injected intravenously with 50 μg BrdU/gram of body weight 3 hours before sacrifice. Embryos were fixed and embedded in paraffin as described above to obtain transverse sections. BrdU was detected by immunohistochemistry as described (Nowakowski et al., 1989; Selleri et al., 2001) and sections were counterstained lightly with hematoxylin and eosin. Monoclonal anti-BrdU was purchased from Neo Markers. All BrdU-positive (dark brown) and negative (blue) nuclei were counted over various sections. Five different sections (per axial level) containing sclerotome and vertebral anlage were analyzed for each wildtype (WT) and $Pbx1^{-/-};Pbx2^{+/-}$ littermate embryo; this comparison was performed on three embryos for each genotype per gestational day (E9.5, E11.5, E12.5). Sections were digitized using an Eclipse E600 microscope (Nikon). For each section, outlines of the notochord and sclerotome areas were traced manually, corresponding areas were computed, and positive and negative cells counted digitally (Stereo Investigator Software Package, Version 5.05.4, Micro-brightfield). Approximately 400–600 cells (dependent on the genotype and gestational day analyzed) in total were counted per each section. To compare cell densities between WT and mutant embryos, total cell numbers (both positive and negatively stained nuclei) were counted within a standard area encompassing the sclerotome and then

normalized using this area measurement. Next, they were compared using Student's *t*-tests as described elsewhere (Capellini et al., 2006).

Anti-phospho H3 labeling—Embryos were treated and sectioned according to the protocol described above for section *in situ* hybridization. Slides were rinsed in PBS and incubated first with PBS and goat serum, and later with rabbit-polyclonal anti-phospho histone H3 (pHH3; Upstate Biotechnology)(1:1000) O/N. The next day, slides were incubated with an anti-Rabbit biotinylated IgG secondary antibody (Jackson ImmunoResearch) diluted 1:500 in PBS at RT for 30 min, then treated with Streptavidin conjugated peroxidase ABC kit (Vector Laboratories, Cat# SA-5004), and finally signal was detected using diaminobenzidine (DAB) substrate.

Caspase3 apoptosis assays

Caspase3 antibody staining was used to distinguish apoptotic cells from non-apoptotic cells in compound *Pbx1/Pbx2* mutant versus littermate WT embryos. Initially, paraffin embedded embryos were sectioned to 10 μm using a Leica microtome and treated for immunohistochemistry as described above. After blocking, the Rabbit anti-Caspase3 (R&D Systems, Cat# AF-835) primary antibody (Biogenesis) was diluted 1:2000 in PBS/0.1% TritonX-100 and applied at 4°C O/N. The sections were next incubated with biotinylated Goat anti-Rabbit IgG secondary antibody (Vector Laboratories, Cat# BA-1000) diluted 1:500 in PBS at RT for 30 min, and the signal was detected using HRP-Streptavidin (Vector Laboratories, Cat# SA-5004) as described above. Three embryos per genotype were examined at each gestational time point including the key controls, $Pbx1^{-/-}; Pbx2^{+/+}$ and $Pbx1^{+/-}; Pbx2^{-/-}$.

Results

TALE homeodomain proteins are present in the somitic mesoderm, the notochord, and the surrounding mesenchyme during mid-gestation

Previous studies have uncovered the presence of *Pbx1* and *Pbx2* in the somitic mesoderm and the LPM of developing embryos (Capellini et al., 2006; Schnabel et al., 2001). *In situ* hybridization, as performed here, revealed that PBC- and MEIS-encoding genes were variably expressed in the notochord and condensing pre-vertebral mesenchyme from E10.5–E12.5 (Suppl. Fig. 1). Specifically, *Pbx1* was strongly expressed in the developing notochord and detectable in the surrounding mesenchyme (Suppl. Fig. 1A–C) and *Pbx2* was present, albeit at lower levels, in the notochord (Suppl. Fig. 1D–F). In addition, *Pbx2* was diffusedly expressed in the adjacent mesenchyme, in agreement with previous results indicating widespread expression of *Pbx2* throughout the embryo (Selleri et al., 2004). Conversely, *Pbx3* expression levels in the notochord and surrounding mesenchyme were either extremely low or undetectable (Suppl. Fig. 1G–I). Despite the varied expression of these *Pbx* genes in the notochord and mesenchyme, all three were highly expressed in the ventral columns of the spinal cord (Suppl. Fig. 1). *Meis* genes were also expressed in the spinal cord and at higher levels in the ventral horns (Suppl. Fig. 2). However, unlike *Pbx1*, both *Meis1/Meis2* were expressed at relatively lower levels in the notochord and adjacent somitic mesoderm and mesenchyme (Suppl. Fig. 2A–F), while *Meis3* was absent from these tissues (Suppl.

Fig. 2G–I). Although mid-thoracic level transverse sections are shown depicting *Pbx* and *Meis* expression patterns, similar results were obtained at all axial levels (data not shown). The above results for *Pbx* and *Meis* gene expression were corroborated with immunohistochemistry using Pbx- and Meis-specific antibodies from E10.5 to E12.5 (see Fig. 1A; Pbx1 localization at E10.5 is not shown).

To determine if Pbx protein localization persisted in the notochord and condensing mesenchyme of the vertebral bodies, additional immunohistochemistry at E13.5 (i.e., the gestational day of lethality of compound *Pbx1/Pbx2* mutants reported below) was performed. Indeed, Pbx1 and Pbx2 proteins persisted in both the notochord and condensing mesenchyme of the vertebral bodies and were present in the forming perichondria (Fig. 1B). Also, consistent with *Pbx3* expression patterns and protein localization at earlier gestational days (Suppl. Fig. 1G–I and Fig.1A), Pbx3 protein, while strongly present in the ventral horns of the spinal cord, was undetectable in the notochord, the condensing mesenchyme of the vertebral bodies, and the perichondria (Fig. 1B).

Loss of *Pbx1/Pbx2* causes drastic post-cranial axial skeletal defects

To investigate whether Pbx1 and Pbx2 have roles in the developing primaxial and abaxial skeleton, compound *Pbx1/Pbx2* mutants were generated (see methods). Skeletal and/or soft tissue abnormalities were evident only in $Pbx1^{-/-};Pbx2^{+/+}$, $Pbx1^{-/-};Pbx2^{+/-}$, and $Pbx1^{-/-};Pbx2^{-/-}$ embryos. Since $Pbx1^{-/-};Pbx2^{-/-}$ embryos die at E9.5/10 due to multiple organogenesis defects (Capellini et al., 2006) our analyses focused on $Pbx1^{-/-};Pbx2^{+/-}$ (hereafter, *Pbx1/2 mutant*) embryos, which survive until E13.5, a gestational time-point sufficient to investigate the early development of the axial skeleton.

Pbx1/2 mutant embryos exhibited drastic exacerbations of $Pbx1^{-/-}$ axial skeletal defects (Selleri et al., 2001) at E13.5 (Fig. 2). Unlike WT (Fig. 2A–C, J,M), single $Pbx1^{-/-};Pbx2^{+/+}$ embryos displayed several vertebral and rib defects, such as loss of identities of cervical vertebrae number 1 (hereafter, C1) and C2 (Fig. 2D–F), proximal-distal shortening of ribs that lacked their most ventral domains, and fusion of ribs at the midshaft (Fig 2K,N). Interestingly, despite the lack of vertebral and rib defects in $Pbx1^{+/+};Pbx2^{-/-}$ and $Pbx1^{+/-};Pbx2^{-/-}$ embryos, *Pbx1/2 mutant* embryos displayed more severe defects in those axial domains affected by the loss of *Pbx1* alone (Fig. 2G–I, L,O) and significant malformations at additional axial levels (Fig. 2L,T,U). Specifically, in the cervical region, unlike WT (Fig. 2B–C), *Pbx1/2 mutant* C1 and C2 were more rudimentary in appearance versus $Pbx1^{-/-};Pbx2^{+/+}$ C1 and C2 (Fig. 2E–F) and lost all features typical of these vertebral elements (Fig. 2H–I). Additionally, in the *Pbx1/2 mutant* the remaining cervical vertebrae exhibited thinned transverse processes, which gave the appearance of a loss of identity. Therefore, based on morphological comparisons, the transition from the cervical to thoracic vertebrae was poorly defined at this developmental stage (Fig. 2H–I). In the thoracic region, unlike in WT (Fig. 2J,M) and $Pbx1^{-/-};Pbx2^{+/+}$ (Fig. 2K,N) embryos, all vertebral centra were more flattened and medial-laterally attenuated in *Pbx1/2 mutant* embryos (Fig. 2L,O). The rib defects observed in $Pbx1^{-/-};Pbx2^{+/+}$ embryos (Fig. 2K,N) were more severe in *Pbx1/2 mutant* embryos, as individual elements appeared as extremely shortened, rudimentary cartilage condensations (Fig. 2L,O). In addition, the rib cartilages for rib #1 and

#13 were barely detectable. When coupled with the general rudimentary morphology of the vertebrae, as in the cervical region, the transition from thoracic to lumbar segments was also difficult to discern. In the lumbar-sacral and caudal regions, transverse processes were markedly attenuated or flattened in *Pbx1/2 mutant* embryos (Fig. 2T–U), unlike in WT (Fig. 2P–Q) and *Pbx1*$^{-/-}$;*Pbx2*$^{+/+}$ (Fig. 2R–S) embryos and the overall posterior regionalization of the vertebral column was difficult to demarcate.

To more deeply characterize the axial defects present in *Pbx1/2* mutant embryos, detailed dissections of isolated vertebral elements were performed (Fig. 3). At E13.5, *Pbx1/2 mutant* C1 and C2 were fused and their transverse processes were more acutely angled (Fig. 3A, right, all views) compared to WT C1 and C2 vertebrae (Fig. 3A, left, all views). Furthermore, due to this fusion, a distinguishable dens (odontoid process) was absent from the mutant C2 (Fig. 3A, right, ventral view) when compared to WT (Fig. 3A, left, ventral view). Finally, in the *Pbx1/2 mutant* the transverse processes were markedly thinned and lacked the anlagen of the anterior and posterior tubercles (Fig. 3A, right, lateral view). Several of the alterations present in the most rostral cervical vertebrae of *Pbx1/2 mutant* embryos were also apparent in more caudal cervical vertebrae, such as C4. For example, an acute angulation (Fig. 3A, right, cranial view) and thinning (data not shown) of the transverse processes were present, unlike in WT (Fig. 3A, left, cranial view). Additionally, unlike WT C4 (Fig. 3A, left, cranial view), the groove for the vertebral artery was absent and the centrum was more rounded (Fig. 3A, right, cranial view), similar to that of thoracic vertebrae (compare C4 *Pbx1/2 mutant* cranial view to T3 WT cranial view), and potentially suggestive of a homeotic transformation. Lastly, the vertebral centrum of C4 (as well as other, more caudal, cervical vertebrae) was rostral-caudally flattened (Fig. 3A, right, ventral view) compared to WT (Fig. 3A, left, ventral view).

Defects were also present in *Pbx1/2 mutant* thoracic vertebrae, as represented here by T3, which possessed more acutely angled and attenuated transverse processes, a markedly reduced rostral-caudal thickness of the vertebral centrum anlagen, and loss of more distal rib structures (Fig. 3B, right, all views) when compared to WT (Fig. 3B, left, all views). In addition, its centrum was more rounded (Fig. 3B, right, cranial view) than in WT (Fig. 3B, left, cranial view). Cartilage defects were also present in the lumbar region, as represented here by L3 (Fig. 3C, all views). Specifically, its centrum was more rounded (Fig. 3C, right, cranial view) and more markedly rostral-caudally flattened (Fig. 3C, right, ventral and lateral views) than in WT (Fig. 3C, left, all views). Furthermore, in a similar pattern to that observed for more rostral vertebrae, the transverse processes of the *Pbx1/2 mutant* L3 were extremely thinned and missing superior, middle, and inferior turbercles (Fig. 3C, right, lateral view) compared to WT (Fig. 3C, left, lateral view). In this manner, both the thoracic and lumbar vertebrae more similarly resembled one another than their WT axial counterparts. Overall, despite the persistence of one *Pbx2* allele, the morphology of the vertebral column in *Pbx1/2 mutant* embryos appeared homogeneous.

Pbx1/2 mutant axial defects are not associated with alterations in cellular proliferation and apoptosis in the notochord and surrounding mesoderm and mesenchyme

To examine if detectable changes in cellular behaviors in the notochord and surrounding mesenchyme were responsible for the observed axial skeletal defects, tissue histology, cell density, cell proliferation, and apoptosis assays were performed on *Pbx1/Pbx2* compound mutant and WT embryos from E9.5 to E13.5 (Fig. 4A, Suppl. Fig. 3, and data not shown). Hematoxylin and Eosin staining on E13.5 transverse sections revealed that in *Pbx1/2 mutant* embryos the structure of the notochord and of the adjacent mesenchymal condensation were relatively normal compared to WT (Fig. 4A and Suppl. Fig. 3A). Visual and statistical examination of cell densities between WT and *Pbx1/2 mutant* embryos from E9.5 to E13.5 revealed that at each gestational day analyzed *Pbx1/2 mutant* embryos possessed lower densities of cells around the notochord compared to WT controls (e.g., at E11.5, $p < 0.01$) (Fig. 4A and Suppl. Fig. 3A–C). The lower cell density observed in *Pbx1/2 mutant* embryos could not be causally related to detectable changes in cell proliferation or apoptosis at these gestational days (see below). Furthermore, this difference could not be attributed to edema. Indeed, while edema was slightly present at E12.5 and more markedly present at E13.5 (as previously reported in Capellini et al., 2006), it was barely detectable from E9.5 to E11.5 (Fig. 4A, Suppl. Fig. 3A–C, and data not shown). To examine if the loss of *Pbx1/Pbx2* affected rates of cellular proliferation in the notochord and adjacent mesenchyme, both BrdU (Fig. 4A and Suppl. Fig. 3B) and anti-phospho H3 (data not shown) assays were performed from E9.5 to E12.5. Despite the observed differences in cellular density, at all gestational days (represented here by transverse sections at E11.5 and E12.5), no differences in BrdU- or H3-positive cells were detected in *Pbx1/2 mutant* versus WT embryos (Fig. 4A and Suppl. Fig. 3B). Likewise, analyses of apoptosis using Caspase3 assays at E9.5–E13.5 revealed no differences between *Pbx1/2 mutant* and WT embryos (Fig. 4A and Suppl. Fig. 3C). Overall, the observed abnormalities in axial skeletal morphology (Figs. 2–3) and histology (Fig. 4A and Suppl. Fig. 3A) in *Pbx1/2 mutant* embryos could not be explained by alterations in proliferation or apoptosis in the somitic mesoderm, notochord, and surrounding mesenchyme.

Pbx1/2 mutant vertebral defects are coupled with shifts in hindlimb position along the embryonic axis

Interestingly, unlike WT and $Pbx1^{-/-};Pbx2^{+/+}$ embryos, *Pbx1/2 mutant* embryos also displayed rostral shifts in hindlimb position (Fig. 5A and data not shown). Specifically, at E13.5, the pelvic girdle of *Pbx1/2 mutant* embryos was positioned laterally approximately 2–4 vertebrae caudal to the last rib-bearing thoracic vertebra. In contrast, in WT littermates, the pelvic girdle resided laterally, but approximately 5–6 vertebrae caudal to the last thoracic vertebra. Due to the early lethality at E13.5 of these mutants, before sacral induction occurs (Kaufman, 1992), it was not possible to ascertain the exact position of the pelvic girdle and hindlimb with respect to the lumbar-sacral boundary. However, in agreement with this rostral hindlimb shift, at earlier gestational days (e.g. E10.5) the position of the hindlimb bud was found to be shifted rostrally by approximately 1–3 somites (Table 1). Conversely, the position of the forelimb bud (and skeleton) of *Pbx1/2 mutant* embryos was found to be usually unchanged compared to WT, although on rare occasion a slight forelimb shift was also observed (Table 1 and Fig. 6A).

To ascertain if the position of the hindlimb bud was shifted with respect to their developing peripheral nerves, immunohistochemical staining with an anti-2H3 neurofilament antibody was performed at E11.5 (data not shown) and E12.25 (Fig. 5B). First, it was uncovered that the *Pbx1/2 mutant* hindlimb bud was rostrally shifted and the distance between forelimb and hindlimb buds was reduced compared to WT (Fig. 5B). Second, as detected by this staining, it was evident that neurogenesis was compromised in the more posterior domains of the *Pbx1/2 mutant* embryo. Indeed, developing peripheral nerves entering the WT hindlimb were not detectable in the *Pbx1/2 mutant* hindlimb bud (Fig. 5B).

Finally, as compound *Hox9* paralogous mutants have been recently shown to possess posterior hindlimb shifts (McIntyre et al., 2007; Wellik, 2007), *in situ* hybridization with a *Hoxd9* probe (as well as other *Hox* probes, see below) was performed to determine if alterations in its expression pattern were associated with the hindlimb rostralization in *Pbx1/2 mutant* embryos. Indeed, the anterior boundary of *Hoxd9* expression was rostralized by at least three somites and up-regulated in the LPM in mutants, compared to somite-matched WT embryos (Fig. 5C).

Pbx1/2 mutant vertebral defects are associated with rostral shifts in the expression of *Hox* genes and down-regulation of Polycomb group genes, *Bmi/Eed*, along the embryonic axis

Given the reported roles of the spatio-temporal *Hox* activation (Dubrulle et al., 2001) on vertebral patterning (reviewed in Wellik, 2007) and hindlimb bud positioning (Cohn et al., 1997), additional whole-mount *in situ* hybridizations were performed on *Pbx1/Pbx2* mutant and WT embryos using other *Hox* probes (*Hoxa4, Hoxb5, Hoxb8, Hoxc6*, and *Hoxd3*). For all *Hox* genes analyzed, in contrast to their WT expression, PM expression was shifted rostrally by 1–3 somites in somite-matched *Pbx1/2 mutant* embryos at E10.5–E10.75 (Fig. 6A displays representative results for *Hoxd3, Hoxb8*, and *Hoxc6*). These rostral shifts occurred independently of changes in neuroectodermal *Hox* expression, which remained relatively unperturbed in mutant embryos, and resembled the pattern described above for *Hoxd9* (Fig. 5C). Overall, these findings are concurrent with the observed defects in vertebral morphology as well as the rostral shifts in hindlimb bud positioning (Table 1) in *Pbx1/2 mutant* embryos.

Recently, it has been uncovered that the loss of the repressive effects of Polycomb group protein function, as reported in *Bmi* and *Eed* single and compound mutant mice, leads to rostral shifts in *Hox* gene expression and alterations in vertebral identity and morphology (Kim et al., 2006). To ascertain if shifts in *Hox* gene expression in *Pbx1/2 mutant* embryos were concurrent with perturbations in either *Bmi* and/or *Eed* gene expression, *in situ* hybridizations with specific Polycomb probes were performed. Indeed, the expression of both Polycomb group genes was severely reduced to absent in *Pbx1/2 mutant* embryos at E10.5 and E11.5 (Fig. 6B). Specifically, at E10.5, despite their widespread expression in most embryonic tissues (Kim et al., 2006), which accounts for low-level background signal, both *Bmi/Eed* transcript levels were reduced in the somites of *Pbx1/2 mutant* embryos across the entire rostral-caudal embryonic axis and such reductions were more severe posteriorly (Fig. 6B and data not shown). The perturbation in the *Bmi/Eed* expression

worsened at E11.5, as weaker and more diffused signal was detected along posteriorly located somites in *Pbx1/2 mutant* embryos (Fig. 6B and data not shown).

Pbx1/2 mutant axial skeletal defects are not associated with perturbed expression of notochord markers

To address potential roles of *Hox* genes in the notochord during early axial morphogenesis, *in situ* hybridization of selected *Hox* genes, such as *Hoxb1, Hoxb2, Hoxc6, Hoxd9*, as well as the *Hox* genes mentioned above, was performed on WT embryos from E9.5 to E12.5. Unlike for *Hox* gene expression in the zebrafish notochord (Prince et al., 1998), very weak to undetectable expression was observed for the above-mentioned *Hox* genes in the mouse notochord (data not shown). These data support the notion that an alteration of *Hox* gene expression in the PM, but not in the notochord, of *Pbx1/2 mutant* embryos underlies their vertebral defects.

Given the demonstrated roles of notochord signaling on somite differentiation and morphogenesis of the axial skeleton (Cleaver and Krieg, 2001; Pourquie et al., 1993; Watterson et al., 1954), *in situ* hybridization using notochord-specific markers such as *Brachyury, Noggin*, and *Shh* was performed on transverse sections of *Pbx1/2 mutant* and WT embryos at different axial levels (cervico-thoracic, thoracic-lumbar, and lumbar-sacral) from E11.5–E13.5. At all gestational days analyzed and at all axial levels, the expression of these notochord markers remained unperturbed in *Pbx1/2 mutant* embryos (Fig. 4B; *Noggin* data not shown). Furthermore, as previously reported (Capellini et al., 2006), *Shh* expression remained normal in the notochord in *Pbx1/2 mutant* embryos at E9.5–E10.5.

Pbx1/2 mutant axial skeletal defects are associated with perturbation of *Pax1/Pax9* expression in early somites and sclerotome, but not with alterations in mesenchymal and cartilage cell differentiation

Recent research has demonstrated the roles of *Pax1/Pax9* in somite formation, sclerotomal morphogenesis and differentiation, and development of the posterior vertebrate axial skeleton (Peters et al., 1999; Rodrigo et al., 2003). To ascertain whether the expression of *Pax1/Pax9* was reduced during somite formation, whole mount *in situ* hybridization was performed on WT and late surviving $Pbx1^{-/-};Pbx2^{-/-}$ mutant embryos spanning gestational days E10–E10.75 (i.e., time-points just prior to their demise). $Pbx1^{-/-};Pbx2^{-/-}$ embryos had in general significantly fewer somites; and indeed in those somites that did form, the expression of *Pax1/Pax9* was absent, specifically when compared to WT control and littermate embryos at earlier as well as similar gestational days (Fig. 7A). Interestingly, *Pax9* remained expressed in the caudal pre-somitic mesoderm of these mutants despite the absence of both *Pax9* and *Pax1* in mature somites, indicating that the initiation steps in somite formation may have occurred normally (Fig. 7A). Detailed analyses of these events were hampered in *Pbx1/Pbx2* double homozygous mutants by their early lethality and global malformations.

To explore whether the expression of *Pax1/Pax9* was altered in *Pbx1/2 mutant* embryos at later stages of sclerotomal morphogenesis, both whole-mount and section *in situ* hybridizations were performed at E11.5. Due to the observed axial shifts in hindlimb bud

positioning in *Pbx1/2 mutant* embryos, section *in situ* hybridizations were performed on multiple axial levels from both WT and *Pbx1/2 mutant* embryos and equivalent axial levels were carefully compared. In whole-mount embryos (Fig. 7B–C), both *Pax1* and *Pax9* expression was down-regulated along the embryonic axis, although the latter was not as reduced as the former (Fig. 7C). Specifically, *Pax1* expression was down-regulated in lumbar-sacral domains, as well as along the flank and in both fore- and hindlimbs (albeit more reduced in the anterior hindlimb than forelimb) (Fig. 7B). Interestingly, *Pax1* expression was also spatially altered in the sclerotome of *Pbx1/2 mutant* embryos at all gestational days analyzed, as shown by section (Fig. 7B). The observed spatial perturbation in *Pax1* expression became more diffused throughout the sclerotome at the lumbar-sacral (hindlimb) axial level (Fig. 7B, middle). At E11.5, the down-regulation of these genes occurred in the noticeable absence of edema, which only became evident after E12.5 in *Pbx1/2 mutant* embryos. Furthermore, analysis of additional genes such as *Sox9* (Wright et al., 1995) and *Col2a1* (Cheah et al., 1991) at E12 and E13 (Fig. 7D, right), revealed relatively normal patterns of expression in *Pbx1/2 mutant* embryos despite the presence of slight edema in their expression domains (see below). The observations that *Pax1/Pax9* are down-regulated and spatially diffused in the sclerotome of *Pbx1/2 mutant* embryos sheds light on the genetic control of *Pax* by *Pbx* in this tissue; specifically since *Pbx1/2 mutants*, unlike $Pbx1^{-/-};Pbx2^{-/-}$ embryos, possess relatively normal somite numbers and morphology during mid-gestation. Finally, despite the perturbation in *Pax1* and *Pax9* spatial distribution, expression of *Bapx1*, a known target of these *Pax* genes in the axial mesoderm (Rodrigo et al., 2003), remained relatively unperturbed in *Pbx1/2 mutant* embryos (data not shown).

To ascertain if the observed skeletal defects in *Pbx1/2 mutant* embryos were associated with disruptions in mesenchyme of the sclerotome and cartilage cell differentiation in all domains of the forming vertebrae, additional whole-mount and section *in situ* hybridization were performed at E12 to E13 using *Sox9* (Wright et al., 1995), *Noggin* (Valenzuela et al., 1995), and *Col2a1* (Cheah et al., 1991), markers of this differentiation process (Fig. 7D and data not shown). By whole-mount *in situ* hybridization, as shown at E12, both *Sox9* and *Col2a1* remained similarly expressed in all vertebral domains in both WT and *Pbx1/2 mutant* embryos (Fig. 7D, left). Expression of *Noggin* also remained unchanged (data not shown). Noticeable differences were only evident for *Sox9* in the pre-rib mesenchyme, as in *Pbx1/2 mutant* embryos its expression was absent, coincident with the presence of rudimentary ribs in these embryos. In order to further ascertain whether cellular differentiation occurred normally in *Pbx1/2 mutant* embryos in all vertebral domains (i.e., vertebral centra, laminae, and neural arches), *in situ* hybridization on multiple axial levels from both WT and *Pbx1/2 mutant* embryos was performed to avoid poor matching of sections due to the observed axial shifts in hindlimb bud positioning in the latter genotype. At both E12 and E13, only minor differences were observed in the expression of *Sox9* in the anterior (thoracic), but not posterior (caudal) mesenchyme that gives rise to the vertebral centra, whereas *Sox9* remained normally expressed in the notochord and all condensations that give rise to the lamina and neural arches (Fig. 7D, right). At these same gestational days, *Noggin* and *Col2a1* remained similarly expressed in these domains in comparable sections of WT and *Pbx1/2 mutant* embryos (Fig. 7D, right and data not shown), even at those axial levels where dysmorphologies of the cartilaginous condensations were evident (see *Col2a1* panel).

Overall, mesenchymal and cartilage cellular differentiation, as assessed by these markers, remained relatively unaltered in *Pbx1/2 mutant* embryos.

Discussion

Pbx1/Pbx2 are required in the axial mesoderm for primaxial and abaxial skeletal patterning

Our results establish that, while *Pbx1* is primarily required for patterning of the cervical vertebrae and the distal ribs (Selleri et al., 2001), *Pbx1/Pbx2* share overlapping functions in the development of both the primaxial and abaxial skeleton. As for primaxial domains, when compared to $Pbx1^{-/-}$ embryos, *Pbx1/2 mutant* embryos displayed more severe dysmorphologies in all vertebral compartments, as their vertebrae were hypoplastic and lacked many of the characteristic features of each specific axial region (Figs. 2–3). The vertebral dysmorphologies and the early lethality of *Pbx1/2 mutant* embryos made it difficult to discern if the demarcations between vertebral regions were properly maintained. However, it was evident that at transitions between vertebral segments strong similarities were present in adjacent vertebrae. For example, in *Pbx1/2 mutant* embryos there are at least eight vertebrae in the cervical region that display similar transverse and centra morphologies, while only seven are normally present in WT embryos (Fig. 2). In addition, C4 exhibited transverse and centrum morphologies similar to upper thoracic vertebrae, such as T3 (Fig. 3). Likewise, all lumbar-sacral vertebrae were morphologically similar and together with the rostralization of the hindlimb, these phenotypes may indicate a general shift in lumbar-sacral morphology (Figs 2, 3, and 5). Thoracic patterning and development were also severely compromised in *Pbx1/2 mutant* embryos, as cartilaginous rib rudiments persisted but were heavily truncated distally in abaxial domains (Figs. 2–3). Besides their anatomical location, these rudiments lacked any characteristics that would ascribe them to a specific rib number. In addition, sternal primordia were also absent in the *Pbx1/2 mutant* embryos (data not shown). When these data are taken together, the entire axial vertebral skeleton of *Pbx1/2 mutant* embryos may be considered homogeneous, indicating that its global patterning was disrupted in the absence of *Pbx1/Pbx2*.

As in the limb, except for $Pbx1^{-/-}$ (Selleri et al., 2001), *Pbx1/2 mutant*, and $Pbx1^{-/-};Pbx2^{-/-}$ embryos (Capellini et al., 2006), all other compound *Pbx1;Pbx2* genotypes lacked axial skeletal defects. Furthermore, only *Pbx1/2 mutant* embryos displayed significant alterations in gene expression (see above). These findings highlight the primary role of *Pbx1*, and the critical impact that overlapping *Pbx1/Pbx2* spatio-temporal expression patterns have on axial development. Indeed, the early co-localization of Pbx1/Pbx2 in developing and differentiating somites and in the LPM may be critical in axial skeletal patterning (Fig. 1 and Suppl. Fig. 1). Our data indicate that, unlike the limb, where after initial bud formation *Pbx1/Pbx2* occupy complementary domains (Capellini et al., 2006), *Pbx1/Pbx2* are expressed in overlapping mesodermal (and mesodermal-derived) domains throughout successive stages of vertebral and rib morphogenesis (Fig. 1 and Suppl. Fig. 1). However, in the mesoderm during rostral to caudal patterning of the axial skeleton, Pbx1/Pbx2 function most likely early (i.e., during somite patterning) and reiteratively (see below), while later sclerotomal and cartilage cell differentiation are unaffected in the developing vertebrae of *Pbx1/2 mutant* embryos (Fig. 7D). Differences were only evident in the mesenchymal

condensations of developing ribs, as shown by the loss of *Sox9* expression in these domains in *Pbx1/2 mutant* embryos (Fig. 7D), not excluding a possible role of Pbx at later stages during rib morphogenesis and differentiation. Tissue-specific inactivation of *Pbx1* on a *Pbx2*-deficient background will help clarify Pbx roles in these domains.

Finally, we have revealed that even though *Pbx1/Pbx2* are expressed in the mouse notochord, their compound loss does not influence its morphological development or the expression of notochord-specific markers (Fig. 4). These data support our hypothesis that *Pbx1/Pbx2* function in the mesoderm during primaxial and abaxial patterning.

Pbx roles in vertebral patterning are partially mediated by their genetic control of Polycomb group gene expression in the PM

We observed a striking down-regulation of the expression of *Bmi/Eed* in *Pbx1/2 mutant* embryos (Fig. 6B). The proteins that these genes encode function additively, in separate Polycomb complexes during the “maintenance phase” of *Hox* expression boundaries, to repress *Hox* gene transcription in somites rostral to the anterior limit of *Hox* expression (Kim et al., 2006). Indeed, single $Bmi^{-/-}$, and $Eed^{-/-}$ mutants and several compound *Bmi;Eed* mutants display rostralizations of *Hox* gene expression domains, and exhibit homeotic transformations and alterations in vertebral patterning (Faust et al., 1995; 1998; Kim et al., 2006; Lessard et al., 1999; van der Lugt et al., 1994). Importantly, these patterning alterations were found across all axial levels and were dosage-dependent (Kim et al., 2006; Fig. 2). When taken in this context, *Pbx* may control *Hox* spatial distribution indirectly, via their hierarchical control of the Polycomb group genes. Accordingly, as shown in Figure 8 (A–B), as a consequence of *Pbx* loss, *Bmi/Eed* are down-regulated along the rostral to caudal axis in the *Pbx1/2 mutant* and their repressive effects relieved, leading to the rostralization of *Hox* expression boundaries during somite and sclerotomal differentiation.

While *Pbx* genetically control Polycomb, the malformations in *Pbx1/2 mutant* embryos are more extreme than those observed in single and compound Polycomb or *Hox* mutants. Therefore, Pbx likely control additional factors in axial skeletal development. Importantly, Pbx proteins also act as cofactors for Hox members (Hox1–10), and by doing so they increase the DNA binding specificity and selectivity of Hox at target genes (reviewed by Mann and Affolter, 1998; Mann and Chan, 1996; Moens and Selleri, 2006). Accordingly, the loss of Pbx may result in an overall decrease in Hox functionality at all target genes across every region of the axial skeleton, likely leading to the overall loss of identity of all vertebrae.

As mentioned, we have also found that the rostral-most expression domains of all analyzed *Hox* genes representing different paralogous groups (*Hox3, 4, 5, 6, 8, 9*) spanning all four *Hox* clusters are shifted rostrally, typically by at least 2 somites in *Pbx1/2 mutant* embryos (Fig. 6A and 8B). Hox roles in primaxial (Burke et al., 1995; Iimura and Pourquie, 2006; 2007; Krumlauf, 1994) and abaxial patterning (McIntyre et al., 2007; Wellik, 2007) have been extensively documented. Knockout mice harboring null mutations for single and multiple paralogous *Hox* genes demonstrate that different paralogs pattern specific segments of the vertebral column and ribs and that partial functional redundancy exists between

paralogous (and between non-paralogous) members (Iimura and Pourquie, 2007; Wellik, 2007). For example, compound mutants for *Hox4* group paralogs display additive changes in cervical vertebral morphology dependent on *Hox* dosage (Horan et al., 1995), while in mice lacking *Hox10* function (i.e., in which *Hoxa10, Hoxc10*, and *Hoxd10* have been deleted), distinct lumbar vertebrae do not form (Wellik and Capecchi, 2003). Given that *Pbx1/2 mutant* embryos exhibit relatively similar vertebrae lacking axial-level characteristics indicative of their WT counterparts, it cannot be ruled out that the associated rostral shifts in axial *Hox* expression contribute, at least in part, to the etiology of these defects (Fig. 8A–B). Overall, *Pbx* genes may function reiteratively throughout axial development by genetically controlling Polycomb group and *Hox* gene expression, as well as by acting as Hox cofactors (Fig. 8A–B).

Pbx roles in the LPM govern hindlimb positioning

Little is known about the mechanisms by which limb bud position is determined, although evidence for *Hox* roles in limb bud positional specification comes from several single and compound *Hox* mouse mutants. For example, Rancourt et al. (1995) demonstrated that the axial level of scapula formation was shifted in single $Hoxb5^{-/-}$ and compound *Hoxb5;Hoxb6* mutant mice suggesting that forelimb level may also have been altered. McIntyre et al. (2007), on the other hand, found a posterior shift in the axial skeleton of compound homozygous *Hox9* paralogous mutants (i.e., for *Hoxa9/b9/c9/d9*), which placed hindlimbs more caudally than in WT controls. Furthermore, in the chick embryo, Cohn et al. (1997) demonstrated by experimentally altering the expression boundaries of *Hox9* genes (i.e., *Hoxb9, Hoxc9*, and *Hoxd9*) that ectopic limbs formed at different axial levels, although in these experiments shifts in the axial level where limbs normally form were not observed.

Interestingly, associated with *Pbx1/2 mutant* primaxial and abaxial defects, we found that hindlimb position was rostralized by at least two somites at early stages (e.g., E10.5; Table 1) and by two to three vertebrae at later stages (E13.5; Fig. 5). While we previously reported that *Pbx* genes control *Hox* expression in the limb, a derivative of the LPM (Capellini et al., 2006), we now report here that this hierarchical relationship also exists for axial mesodermal tissues and the LPM proper. For example, we found that the loss of *Pbx1/Pbx2* is associated with a rostralization of *Hoxd9* expression in both somites and the LPM (Fig. 5C); and consistent with this potential gain of function, we found that hindlimb location was also rostralized (Fig. 5A–B). This finding is consistent with the posterior shifts in hindlimb bud position described above for *Hox9* loss-of-function mutants. In this regard, the basis for determining hindlimb position may reflect the actions of *Pbx* on *Hox* in the LPM prior to limb induction (see Fig. 8B). At this time, however, *Pbx* may act upstream of other parallel pathways driving limb positioning. For example, after careful re-examination of the reported skeletal defects of single and compound mutants for *Bmi/Eed* (reported in Kim et al., 2006; Fig. 3G), we noticed subtle but noteworthy rostral shifts in hindlimb position. Specifically, despite the posterior transformation of L6 to S1, the location of the sacral attachment of the iliac blades in $Bmi^{-/-}$, $Eed^{-/-}$, and $Bmi^{-/-};Eed^{-/-}$ mutants occurred more rostrally, at the level of L5, rather than at L6 as in the WT. While there is a discrepancy in the degree of hindlimb rostralization between these sets of mutants, at least two points emerge whose consideration may help clarify these differences, as well as the roles of these genes during

axial and limb specification: (1) Kim et al. (2006) reported that the *Eed* mutant allele (*l7Rn5*$^{1989SB/+}$) used to generate *Eed*$^{-/-}$ and *Bmi*$^{-/-}$;*Eed*$^{-/-}$ compound mutants was hypomorphic and when present in its homozygous state led to an ameliorated phenotype compared to a true null allele (*l7Rn5*$^{3345SB/+}$); and (2) The *Pbx1/2 mutant* model used in this paper is heterozygous for *Pbx2*, which results in residual Pbx2 protein and thus implies that the genetic control of *Pbx* on these Polycomb genes is only partially eliminated in *Pbx1/2 mutant* embryos.

Pax1/Pax9 mediate, in part, *Pbx1/Pbx2* roles in the sclerotome and somites, as well as in other mesodermal-derived tissues

Early stages in primaxial development involve the differentiation of the somitic mesoderm into sclerotomal mesenchyme and the maturation of sclerotome into vertebral elements. These processes are mediated by at least two members of the Pax family of transcription factors, Pax1 and Pax9 (Peters et al., 1999; Wallin et al., 1994; Wilm et al., 1998). The functional relationships among these genes during vertebral development is complicated by the finding that in *Pax1* absence, *Pax9* expression is up-regulated and spatially expanded in the sclerotome (Peters et al., 1999), partially rescuing the *Pax1* null vertebral phenotype (Wallin et al., 1994; Wilm et al., 1998). However, in *Pax1*$^{-/-}$;*Pax9*$^{-/-}$ mutants more severe defects in centrum and intervertebral disc morphologies are observed across lumbar, sacral, and caudal domains of the vertebral column.

In *Pbx1/2 mutant* embryos we observed a modest down-regulation and marked spatial perturbation (diffusion) of *Pax1* expression in the sclerotome at all axial levels (Fig. 7B). This pattern was not duplicated for *Pax9*, which while still slightly reduced, persisted in all vertebral axial domains (Fig. 7C). In accordance with Peters et al. (1999), the slight down-regulation of *Pax9* that we observed may reflect the up-regulation of this gene's expression in the sclerotome after *Pax1* down-regulation. Alternatively, the relatively higher *Pax9* expression in *Pbx1/2 mutant* embryos (compared to *Pax1* expression) may result from differences in the regulation of *Pax1 versus Pax9* by *Pbx*. Our findings that both *Pax1* and *Pax9* are down-regulated in other non-axial domains in *Pbx1/2 mutant* embryos and absent in the somites of *Pbx1*$^{-/-}$;*Pbx2*$^{-/-}$ mutants (see Fig. 7A–C) further support our hypothesis of a genetic control of *Pax1* and *Pax9* by Pbx family members (see Fig. 8C). These findings are also consistent with previous reports showing that *Pbx* genes can regulate other Pax family members during embryogenesis, e.g., during thymic development (Manley et al., 2004) and pancreatic islet cell differentiation (Zhang et al., 2006).

Interestingly, from E9.5 to E13.5, we found that the ventro-medial sclerotome in *Pbx1/2 mutant* embryos exhibited significantly lower cellular density, a difference that was not coupled with changes in cell proliferation or apoptosis (Fig. 4A and Suppl. Fig. 3). Conversely, in *Pax1*$^{-/-}$;*Pax9*$^{-/-}$ mutants, similar changes in the density of the sclerotome were reported, but were associated with decreased cell proliferation (E12.5) and increased apoptosis (at E13.5) (Peters et al., 1999). In addition, Rodrigo et al. (2003) discovered that *Bapx1* (a sclerotomal marker) may be a direct transcriptional target of Pax1/Pax9, since its expression was lost in compound *Pax1;Pax9* mutants. In contrast, we found that *Bapx1* expression remained normal in *Pbx1/2 mutant* embryos. These discrepancies may be

attributed to our findings that: (1) in *Pbx1/2 mutant* embryos, *Pax1* and *Pax9* are not completely absent but modestly down-regulated and spatially perturbed to different degrees; and (2) *Pbx1/Pbx2* appear to govern early processes that may pleiotropically influence later morphogenetic events, including cellular density in the developing somites (Fig. 8A; see below).

The genetic control of *Pax1* and *Pax9* by *Pbx1/Pbx2* may also be influenced by Hox themselves. Activation of Hox target genes may be prevented by the loss of their cooperative interactions with Pbx and/or Pax. With regard to the latter, it has been reported that Pax and Hox can form complexes to regulate common target genes (Benassayag et al., 2003; Gong et al. 2007; Plaza et al., 2001). Specifically, Gong et al. (2007) have recently uncovered that the metanephric expression of *Six2* and *Gdnf* requires a complex involving Hox11, Eya1, and Pax2. Furthermore, both Hox and Pax have been shown to physically and genetically interact and to cooperatively regulate downstream target genes in *Drosophila* organogenesis (Benassayag et al., 2003; Plaza et al., 2001). Thus, many of the observed vertebral defects, arising from altered somite and sclerotomal formation in *Pbx1/2 mutant* embryos may result from disruptions in Pax and Hox and their cooperative effects on target gene expression (Fig. 8C).

Summary: Hierarchical, reiterative, and overlapping functions of Pbx genes in multiple developmental processes

We have shown that *Pbx1/Pbx2* have overlapping hierarchical genetic roles in the axial mesoderm that gives rise to the skeletal elements of the vertebral column, as well as ribs, sternum, and clavicle. In the context of the appendicular and girdle defects reported here and in Capellini et al. (2006), these results additionally establish that *Pbx1/Pbx2* genetically regulate the development of all post-cranial skeletal structures. However, *Pbx* genetic control is not limited to skeletal development, as in domains where *Pbx1/Pbx2* are lost, posterior neurogenesis is severely compromised (Fig. 5B). Indeed, a growing body of literature demonstrates that Pbx family members act as hierarchical regulators of many organogenetic processes including, for example, development of hematopoietic (DiMartino et al., 2001; Sanyal et al., 2007), thymic (Manley et al., 2004), splenic (Brendolan et al., 2005), pancreatic (Kim et al., 2002; Zhang et al., 2006), nephrogenic (Schnabel et al., 2003), and adrenal and urogenital (Lichtenauer et al., 2007; Schnabel et al., 2003) systems. In many of these contexts, Pbx has been shown to act as a direct regulator of target gene expression, a control often requiring cooperative interactions with other TALE family members, such as Meis and Prep, as well as Hox proteins. Given the co-localization of many of these partner proteins with Pbx1–3 (Fig. 1 and Suppl. Figs. 1–2), it is likely that the differential regulation of target genes by Pbx requires the formation of context-specific complexes, a process that at this stage is poorly understood. As Pbx, Meis, and Prep global and tissue-specific knockout mice become available, the mechanisms and molecular networks hierarchically regulated by Pbx in many different developmental processes will be clarified.

Supplementary Material

Refer to Web version on PubMed Central for supplementary material.

Acknowledgments

We thank Drs. M. Cleary and F. Blasi for generously providing anti-Pbx, anti-Meis, and anti-Prep antibodies; Drs. T. Lufkin, K. Anderson, K.Chea, M. Capecchi, J.C. Izpisua Belmonte, R. Balling, R. Harland, H. Popperl, A. Schumacher, and A. McMahon for the gift of *Bapx1, Brachyury, Col2a1, Hox, Meis, Noggin, Pax, Pbx*, Polycomb, *Shh* and *Sox9 in situ* probes, respectively. We are grateful to Dr. E. Ferretti for providing *Pbx1/2* mutant embryos; Drs. M. Depew, X. Sun, and J. Verheyden for sharing their neurofilament staining protocols; Dr. K. Manova for technical assistance in apoptosis assays; and Drs. L. Lacy and K. Hadjantonakis for input and many fruitful discussions. T.C. is a recent graduate of the New York Consortium in Evolutionary Primatology and a grateful recipient of the Carole and Morton Olshan Dissertation Fellowship. This work was supported by grants from the National Institutes of Health (HD43997 and DE18031 to L.S. and HD050704 to A.D.G.) and from the March of Dimes and Birth Defects Foundation (Grant #6-FY03-071 to L.S.). A.D.G. and L.S. are Irma T. Hirschl Scholars. L.S. is the grateful recipient of an Alice Bohmfalk Charitable Trust research grant and a donation from The Frueauff Foundation.

References

Aubin J, Lemieux M, Moreau J, Lapointe J, Jeannotte L. Cooperation of Hoxa5 and Pax1 genes during formation of the pectoral girdle. Dev. Biol. 2002; 244:96–113. [PubMed: 11900462]

Balling R, Deutsch U, Gruss P. *Undulated*, a mutation affecting the development of the mouse skeleton, has a point mutation in the paired box of Pax 1. Cell. 1988; 55:531–5. [PubMed: 3180219]

Benassayag C, Plaza S, Callaerts P, Clements J, Romeo Y, Gehring WJ, Cribbs DL. Evidence for a direct functional antagonism of the selector genes proboscipedia and eyeless in Drosophila head development. Development. 2003; 130(3):575–86. [PubMed: 12490563]

Berkes CA, Bergstrom DA, Penn BH, Seaver KJ, Knoepfler PS, Tapscott SJ. Pbx marks genes for activation by MyoD indicating a role for a homeodomain protein in establishing myogenic potential. Mol. Cell. 2004; 14:465–77. [PubMed: 15149596]

Brendolan A, Ferretti E, Salsi V, Moses K, Quaggin S, Blasi F, Cleary ML, Selleri L. A Pbx1-dependent genetic and transcriptional network regulates spleen ontogeny. Development. 2005; 132:3113–26. [PubMed: 15944191]

Burglin TR. Analysis of TALE superclass homeobox genes (MEIS, PBC, KNOX, Iroquois, TGIF) reveals a novel domain conserved between Plants and animals. Nucleic Acids Res. 1997; 25:4173–80. [PubMed: 9336443]

Burglin TR. The PBC domain contains a MEINOX domain: coevolution of Hox and TALE homeobox genes? Dev. Genes Evol. 1998; 208:113–6. [PubMed: 9569353]

Burke AC, Nelson CE, Morgan BA, Tabin C. *Hox* genes and the evolution of vertebrate axial morphology. Development. 1995; 121:333–46. [PubMed: 7768176]

Capdevila J, Tsukui T, Rodriquez Esteban C, Zappavigna V, Izpisua Belmonte JC. Control of vertebrate limb outgrowth by the proximal factor Meis2 and distal antagonism of BMPs by Gremlin. Mol. Cell. 1999; 4:839–49. [PubMed: 10619030]

Capellini TD, Di Giacomo G, Salsi V, Brendolan A, Ferretti E, Srivastava D, Zappavigna V, Selleri L. Pbx1/Pbx2 requirement for distal limb patterning is mediated by the hierarchical control of Hox gene spatial distribution and Shh expression. Development. 2006; 133:2263–73. [PubMed: 16672333]

Chalepakis G, Fritsch R, Fickenscher H, Deutsch U, Goulding M, Gruss P. The molecular basis of the *undulated/ Pax-1* mutation. Cell. 1991; 66:873–84. [PubMed: 1889089]

Charite J, de Graaff W, Shen S, Deschamps J. Ectopic expression of Hoxb-8 causes duplication of the ZPA in the forelimb and homeotic transformation of axial structures. Cell. 1994; 78:589–601. [PubMed: 7915198]

Cheah KS, Au PK, Lau ET, Little PF, Stubbs L. The mouse Col2a-1 gene is highly conserved and is linked to Int-1 on chromosome 15. Mamm Genome. 1991; 1(3):171–83. [PubMed: 1797232]

Christ B, Huang R, Scaal M. Formation and differentiation of the avian sclerotome. Anat. Embryol. 2004; 208:333–50. [PubMed: 15309628]

Christ B, Wilting J. From somites to vertebral column. Ann. Anat. 1992; 174:23–32. [PubMed: 1605355]

Cleaver O, Krieg PA. Notochord patterning of the endoderm. Dev. Biol. 2001; 234:1–12. [PubMed: 11356015]

Cohn MJ, Patel K, Krumlauf R, Wilkinson DG, Clarke JD, Tickle C. Hox9 genes and vertebrate limb specification. Nature. 1997; 387:97–101. [PubMed: 9139829]

Condie BG, Capecchi MR. Mice homozygous for a targeted disruption of Hoxd-3 (Hox-4.1) exhibit anterior transformations of the first and second cervical vertebrae, the atlas and the axis. Development. 1993; 119(3):579–95. [PubMed: 7910549]

Deutsch U, Dressler GR, Gruss P. Pax1, a member of a paired box homologous murine gene family, is expressed in segmented structures during development. Cell. 1988; 53:617–25. [PubMed: 2453291]

Dietrich S, Gruss P. *Undulated* phenotypes suggest a role of *Pax-1* for the development of vertebral and extravertebral structures. Dev. Biol. 1995; 167:529–48. [PubMed: 7875377]

Di Giacomo G, Koss M, Capellini TD, Brendolan A, Popperl H, Selleri L. Spatio-temporal expression of Pbx3 during mouse organogenesis. Gene Expr. Patterns. 2006; 6:747–57. [PubMed: 16434237]

DiMartino JF, Selleri L, Traver D, Firpo MT, Rhee J, Warnke R, O'Gorman S, Weissman IL, Cleary ML. The Hox cofactor and proto-oncogene Pbx1 is required for maintenance of definitive hematopoiesis in the fetal liver. Blood. 2001; 98(3):618–26. [PubMed: 11468159]

Dolle P, Izpisua-Belmonte JC, Falkenstein H, Renucci A, Duboule D. Coordinate expression of the murine Hox-5 complex homoeobox-containing genes during limb pattern formation. Nature. 1989; 342:767–72. [PubMed: 2574828]

Dubrulle J, McGrew MJ, Pourquié O. FGF signaling controls somite boundary position and regulates segmentation clock control of spatiotemporal Hox gene activation. Cell. 2001; 106:219–32. [PubMed: 11511349]

Echelard Y, Epstein DJ, St-Jacques B, Shen L, Mohler J, McMahon JA, McMahon AP. Sonic hedgehog, a member of a family of putative signaling molecules, is implicated in the regulation of CNS polarity. Cell. 1993; 75:1417–30. [PubMed: 7916661]

Faust C, Schumacher A, Magnuson T. The eed mutation disrupts anterior mesoderm production in the mouse. Development. 1995; 121:273–85. [PubMed: 7768172]

Faust C, Lawson KA, Schork NJ, Thiel B, Magnuson T. The Polcomb-group gene eed is required for normal morphogenetic movements during gastrulation in the mouse embryo. Development. 1998; 125:4495–506. [PubMed: 9778508]

Favier B, Dolle P. Developmental functions of mammalian Hox genes. Mol. Human Reprod. 1997; 3(2):115–31.

Ferretti E, Marshall H, Popperl H, Maconochie M, Krumlauf R, Blasi F. Segmental expression of Hoxb2 in r4 requires two separate sites that integrate cooperative interactions between Prep1, Pbx and Hox proteins. Development. 2000; 127:155–66. [PubMed: 10654609]

Fleming A, Keynes R, Tannahill D. A central role for the notochord in vertebral patterning. Development. 2003; 131:873–80.

Frohman MA, Boyle M, Martin GR. Isolation of the mouse Hox-2.9 gene; analysis of embryonic expression suggests that positional information along the anterior-posterior axis is specified by mesoderm. Development. 1990; 110(2):589–607. [PubMed: 1983472]

Gong KQ, Yallowitz AR, Sun H, Dressler GR, Wellik DM. A hox eya-pax complex regulates early kidney developmental gene expression. Mol. Cell. Biol. 2007; 27(21):7661–8. [PubMed: 17785448]

Hendzel MJ, Wei Y, Mancini MA, Van Hooser A, Ranalli T, Brinkley BR, Bazett-Jones DP, Allis CD. Mitosis-specific phosphorylation of histone H3 initiates primarily within pericentromeric heterochromatin during G2 and spreads in an ordered fashion coincident with mitotic chromosome condensation. Chromosoma. 1997; 106:348–60. [PubMed: 9362543]

Horan GSB, Ramirez-Solis R, Featherstone MS, Wolgemuth DJ, Bradley A, Behringer RR. Compound mutants for the paralogous hoxa-4, hoxb-4, and hoxd-4 genes show more complete homeotic transformations and a dose-dependent increase in the number of vertebrae transformed. Genes Dev. 1995; 9(13):1667–77. [PubMed: 7628700]

Hunt P, Wilkinson D, Krumlauf R. Patterning the vertebrate head: murine Hox 2 genes mark distinct subpopulations of premigratory and migrating cranial neural crest. Development. 1991; 112(1):43–50. [PubMed: 1685117]

Hunter CJ, Matyas JR, Duncan NA. Cytomorphology of notochordal and chondrocytic cells from the nucleus pulposus: a species comparison. J. Anat. 2004; 205:357–62. [PubMed: 15575884]

Iimura T, Pourquie O. Collinear activation of Hoxb genes during gastrulation is linked to mesoderm cell ingression. Nature. 2006; 442:568–71. [PubMed: 16760928]

Iimura T, Pourquie O. Hox genes in time and space during vertebrate body formation. Develop. Growth Differ. 2007; 49:265–75.

Jacobs Y, Schnabel CA, Cleary ML. Trimeric association of Hox and TALE homeodomain proteins mediates Hoxb2 hindbrain enhancer activity. Mol. Cell. Biol. 1999; 19:5134–42. [PubMed: 10373562]

Kaufman, MH. Atlas of Mouse Development. Academic Press; New York: 1992.

Kim SK, Selleri L, Lee JS, Zhang AY, Gu X, Jacobs Y, Cleary ML. Pbx1 inactivation disrupts pancreas development and in Ipf1-deficient mice promotes diabetes mellitus. Nat. Genet. 2002; 30(4):430–5. [PubMed: 11912494]

Kim SY, Paylor SW, Magnuson T, Schumacher A. Juxtaposed Polycomb complexes co-regulate vertebral identity. Development. 2006; 133:4957–68. [PubMed: 17107999]

Kmita M, Duboule D. Organizing axes in time and space; 25 years of colinear tinkering. Science. 2003; 301:331–3. [PubMed: 12869751]

Knoepfler PS, Bergstrom DA, Uetsuki T, Dac-Korytko I, Sun YH, Wright WE, Tapscott SJ, Kamps MP. A conserved motif Nterminal to the DNA-binding domains of myogenic bHLH transcription factors mediates cooperative DNA binding with pbx-Meis1/Prep1. Nucleic Acids Res. 1999; 27:3752–61. [PubMed: 10471746]

Koseki H, Wallin J, Wilting J, Mizutani Y, Kispert A, Ebensperger C, Herrmann BG, Christ B, Balling R. A role for *Pax-1* as a mediator of notochordal signals during the dorsoventral specification of vertebrae. Development. 1993; 119:649–60. [PubMed: 8187635]

Krumlauf R, Holland PW, McVey JH, Hogan BL. Developmental and spatial patterns of expression of the mouse homeobox gene, Hox 2.1. Development. 1987; 99:603–17. [PubMed: 2889591]

Krumlauf R. Hox genes in vertebrate development. Cell. 1994; 78:191–201. [PubMed: 7913880]

Lessard J, Schumacher A, Thorsteinsdottir U, Van Lohuizen M, Magnuson T, Sauvageau G. Functional antagonism of the Polycomb-Group genes eed and Bmi1 in hemopoietic cell proliferation. Genes Dev. 1999; 13(20):2691–703. [PubMed: 10541555]

Lichtenauer UD, Duchniewicz M, Kolanczyk M, Hoeflich A, Hahner S, Else T, Bicknell AB, Zemojtel T, Stallings NR, Schulte DM, Kamps MP, Hammer GD, Scheele JS, Beuschlein F. Pre-B-cell transcription factor 1 and steroidogenic factor 1 synergistically regulate adrenocortical growth and steroidogenesis. Endocrinology. 2007; 148(2):693–704. [PubMed: 17082260]

Liem KF Jr, Jessell TM, Briscoe J. Regulation of the neural patterning activity of sonic hedgehog by secreted BMP inhibitors expressed by notochord and somites. Development. 2000; 127:4855–66. [PubMed: 11044400]

Liem, KF., Bemis, WE., Walker, WF., Grande, L. Functional Anatomy of the Vertebrates: An Evolutionary Perspective. Brooks Cole; England: 2001.

Maconochie MK, Nonchev S, Studer M, Chan SK, Popperl H, Sham MH, Mann RS, Krumlauf R. Cross-regulation in the mouse HoxB complex: the expression of Hoxb2 in rhombomere 4 is regulated by Hoxb1. Genes Dev. 1997; 11:1885–95. [PubMed: 9242495]

Manley NR, Selleri L, Brendolan A, Gordon J, Cleary ML. Abnormalities of caudal pharyngeal pouch development in Pbx1 knockout mice mimic loss of Hox3 paralogs. Dev. Biol. 2004; 276(2):301–12. [PubMed: 15581866]

Mann RS, Affolter M. Hox proteins meet more partners. Curr. Opin. Genet. Dev. 1998; 8:423–9. [PubMed: 9729718]

Mann RS, Chan SK. Extra specificity from extradenticle: the partnership between HOX and PBX/EXD homeodomain proteins. Trends Genet. 1996; 12:258–62. [PubMed: 8763497]

McIntyre DC, Rakshit S, Yallowitz AR, Loken L, Jeanotte L, Capecchi MR, Wellik DM. Hox patterning of the vertebrate rib cage. Development. 2007; 134(16):2981–9. [PubMed: 17626057]

Moens CB, Selleri L. Hox cofactors in vertebrate development. Dev. Biol. 2006; 291:193–206. [PubMed: 16515781]

Mukherjee K, Bürglin TR. Comprehensive analysis of animal TALE homeobox genes: new conserved motifs and cases of accelerated evolution. J. Mol. Evol. 2007; 65(2):137–53. [PubMed: 17665086]

Neubuser A, Koseki H, Balling R. Characterization and developmental expression of Pax9, a paired-box-containing gene related to Pax1. Dev. Biol. 1995; 170(2):701–16. [PubMed: 7649395]

Nowakowski RS, Lewin SB, Miller MW. Bromodeoxyuridine immunohistochemical determination of the lengths of the cell cycle and the DNA-synthetic phase for an anatomically defined population. J. Neurocytol. 1989; 18(3):311–8. [PubMed: 2746304]

Nowicki JL, Burke AC. Hox genes and morphological identity, axial patterning versus lateral patterning in the vertebrate mesoderm. Development. 2000; 127:4265–75. [PubMed: 10976057]

Peters H, Wilm B, Sakai N, Imai K, Maas R, Balling R. Pax1 and Pax9 synergistically regulate vertebral column development. Development. 1999; 126:5399–408. [PubMed: 10556064]

Plaza S, Prince F, Jaeger J, Kloter U, Flister S, Benassayag C, Cribbs D, Gehring WJ. Molecular basis for the inhibition of Drosophila eye development by Antennapedia. EMBO J. 2001; 20(4):802–11. [PubMed: 11179224]

Popperl H, Bienz M, Studer M, Chan SK, Aparicio S, Brenner S, Mann RS, Krumlauf R. Segmental expression of Hoxb-1 is controlled by a highly conserved autoregulatory loop dependent upon exd/pbx. Cell. 1995; 81:1031–42. [PubMed: 7600572]

Pourquie O, Coltey M, Teillet MA, Ordahl C, Le Douarin NM. Control of dorsoventral patterning of somitic derivatives by notochord and floor plate. Proc. Natl. Acad. Sci. U.S.A. 1993; 90:5242–6. [PubMed: 8506372]

Prince VE, Price AL, Ho RK. *Hox* gene expression reveals regionalization along the anteroposterior axis of the zebrafish notochord. Dev. Genes Evol. 1998; 208:517–22. [PubMed: 9799433]

Rancourt DE, Tsuzuki T, Capecchi MR. Genetic interaction between hoxb-5 and hoxb-6 is revealed by nonallelic noncomplementation. Genes Dev. 1995; 9:108–22. [PubMed: 7828847]

Rhee JW, Arata A, Selleri L, Jacobs Y, Arata S, Onimaru H, Cleary ML. Pbx3 deficiency results in central hypoventilation. Am. J. Pathol. 2004; 165:1343–50. [PubMed: 15466398]

Robson EJ, He SJ, Eccles MR. A PANorama of PAX genes in cancer and development. Nat. Rev. Cancer. 2006; 6:52–62. [PubMed: 16397527]

Rodrigo I, Hill RE, Balling R, Münsterberg A, Imai K. Pax1 and Pax9 activate Bapx1 to induce chondrogenic differentiation in the sclerotome. Development. 2003; 130:473–82. [PubMed: 12490554]

Sanyal M, Tung JW, Karsunky H, Zeng H, Selleri L, Weissman IL, Herzenberg LA, Cleary ML. B-cell development fails in the absence of the Pbx1 proto-oncogene. Blood. 2007; 109(10):4191–9. [PubMed: 17244677]

Schnabel CA, Selleri L, Jacobs Y, Warnke R, Cleary ML. Expression of Pbx1b during mammalian organogenesis. Mech. Dev. 2001; 100(1):131–5. [PubMed: 11118899]

Schnabel CA, Godin RE, Cleary ML. Pbx1 regulates nephrogenesis and ureteric branching in the developing kidney. Dev. Biol. 2003; 254(2):262–76. [PubMed: 12591246]

Schnabel CA, Selleri L, Cleary ML. Pbx1 is essential for adrenal development and urogenital differentiation. Genesis. 2003; 37(3):123–30. [PubMed: 14595835]

Selleri L, Depew MJ, Jacobs Y, Chanda SK, Tsang KY, Cheah KS, Rubenstein JL, O'Gorman S, Cleary ML. Requirement for Pbx1 in skeletal patterning and programming chondrocyte proliferation and differentiation. Development. 2001; 128:3543–57. [PubMed: 11566859]

Selleri L, DiMartino J, van Deursen J, Brendolan A, Sanyal M, Boon E, Capellini T, Smith KS, Rhee J, Popperl H, Grosveld G, Cleary ML. The TALE homeodomain protein Pbx2 is not essential for development and long-term survival. Mol. Cell. Biol. 2004; 24:5324–31. [PubMed: 15169896]

Sharpe PT, Miller JR, Evans EP, Burtenshaw MD, Gaunt SJ. Isolation and expression of a new mouse homeobox gene. Development. 1988; 102(2):397–407. [PubMed: 2458223]

Smits P, Lefebvre V. *Sox5* and *Sox6* are required for notochord extracellular matrix sheath formation, notochord cell survival and development of the nucleus pulposus of intervertebral discs. Development. 2003; 130:1135–48. [PubMed: 12571105]

Stemple DL. Structure and function of the notochord: an essential organ for chordate development. Development. 2005; 132:2503–12. [PubMed: 15890825]

Toth LE, Slawin KL, Pintar JE, Nguyen-Huu MC. Region-specific expression of mouse homeobox genes in the embryonic mesoderm and central nervous system. Proc. Natl. Acad. Sci. U.S.A. 1987; 84(19):6790–4. [PubMed: 2889208]

Tribioli C, Lufkin T. Molecular cloning, chromosomal mapping and developmental expression of BAPX1, a novel human homeobox-containing gene homologous to Drosophila bagpipe. Gene. 1997; 203:225–33. [PubMed: 9426254]

Valenzuela DM, Economides AN, Rojas E, Lamb TM, Nunez L, Jones P, Lp NY, Espinosa R 3rd, Brannan CI, Gilbert DJ, et al. Identification of mammalian noggin and its expression in the adult nervous system. J. Neurosci. 1995; 15:6077–84. [PubMed: 7666191]

van der Lugt NM, Domen J, Linders K, Van Roon M, Robanus-Maandag E, te Riele H, van der Valk M, Deschamps J, Sofroniew M, van Lohuizen M, et al. Posterior transformation, neurological abnormalities, and severe hematopoietic defects in mice with a targeted deletion of the bmi-1 proto-oncogene. Genes Dev. 1994; 8(7):757–69. [PubMed: 7926765]

Wallin J, Wilting J, Koseki H, Fritsch R, Christ B, Balling R. The role of *Pax-1* in axial skeleton development. Development. 1994; 120:1109–21. [PubMed: 8026324]

Watterson RL, Fowler I, Fowler BJ. The role of the neural tube and notochord in development of the axial skeleton of the chick. Am. J. Anat. 1954; 95:337–99. [PubMed: 14349892]

Wellik DM, Capecchi MR. *Hox10* and *Hox11* genes are required to globally pattern the mammalian skeleton. Science. 2003; 301:363–7. [PubMed: 12869760]

Wellik DM. Hox patterning of the vertebrate axial skeleton. Dev. Dyn. 2007; 236(9):2454–63. [PubMed: 17685480]

Wilkinson DG, Bhatt S, Herrmann BG. Expression pattern of the mouse T gene and its role in mesoderm formation. Nature. 1990; 343:657–9. [PubMed: 1689462]

Wilm B, Dahl E, Peters H, Balling R, Imai K. Targeted disruption of *Pax1* defines its null phenotype and proves haploinsufficiency. Proc. Natl. Acad. Sci. U.S.A. 1998; 95:8692–7. [PubMed: 9671740]

Wright E, Hargrave MR, Christiansen J, Cooper L, Kun J, Evans T, Gangadharan U, Greenfield A, Koopman P. The Sry-related gene *Sox9* is expressed during chondrogenesis in mouse embryos. Nat Genet. 1995; 9:15–20. [PubMed: 7704017]

Zhang X, Rowan S, Yue Y, Heaney S, Pan Y, Brendolan A, Selleri L, Maas RL. Pax6 is regulated by Meis and Pbx homeoproteins during pancreatic development. Dev. Biol. 2006; 300:748–57. [PubMed: 17049510]

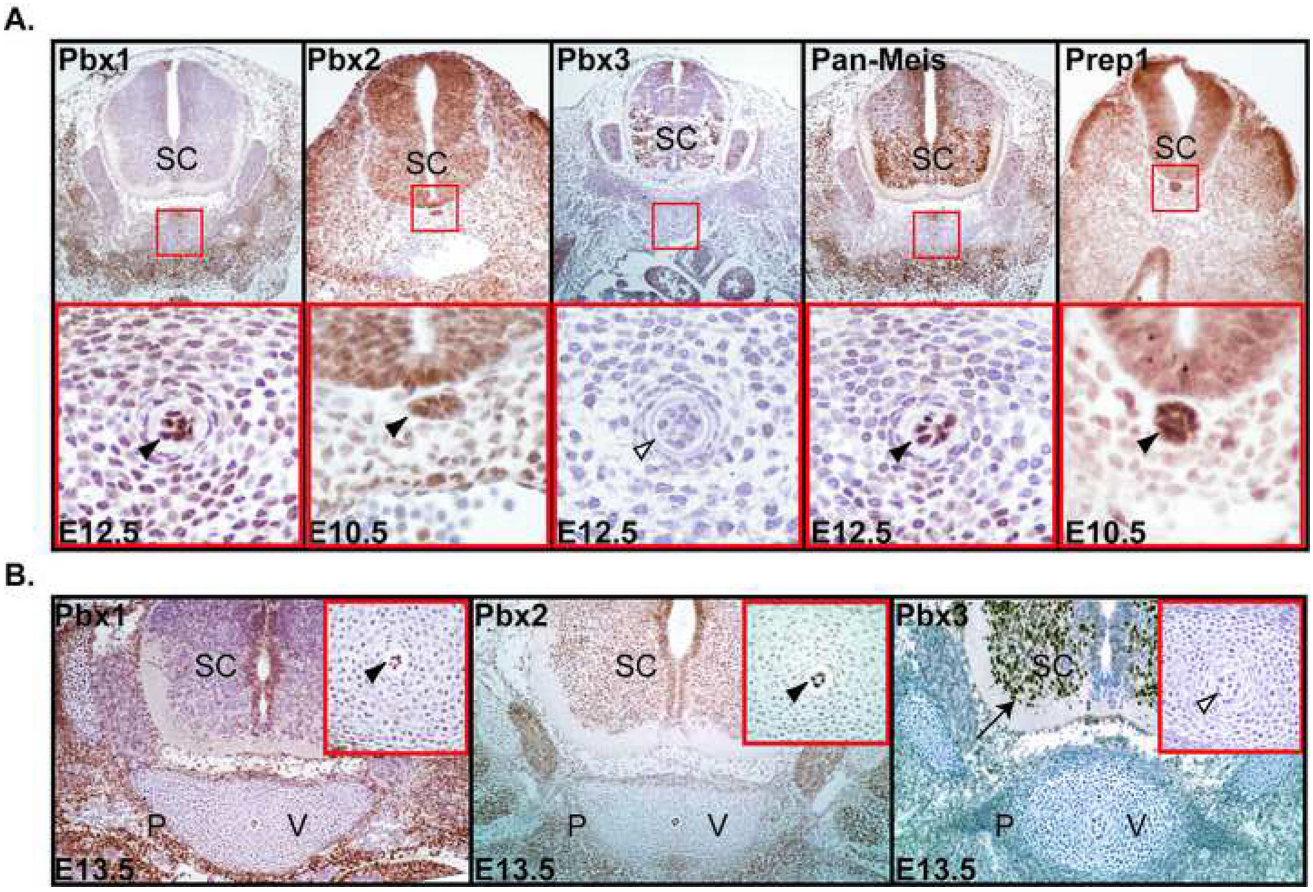

Figure 1. Localization of Pbx and Meis/Prep proteins during notochord and vertebral development

Colocalization of Pbx and Meis/Prep at each gestational day is shown in the 10× view (top panels in A and left panels in B) and the 40× red insets (bottom panel in A and right panels in B). (A) Pbx and Meis proteins are present in the notochord and vertebral anlagen throughout mid-gestation as demonstrated by immunohistochemistry on mid-thoracic transverse sections at E10.5 and E12.5. While at these gestational days Pbx1, Pbx2, Meis and Prep1 colocalize (black arrowheads) in the notochord and also in the adjacent mesenchyme, Pbx3 is absent or present at very low levels in these tissues (empty black arrowhead). (B) At E13.5, Pbx1/Pbx2 colocalize (black arrowheads, red inset) in the notochord as well as in the early vertebral cartilage, while Pbx3 levels remain very low or absent in the latter tissues (empty black arrowhead), as compared to its high levels in the spinal cord (black arrow). P, perichondrium; SC, spinal cord; V, vertebra. Dorsal (top).

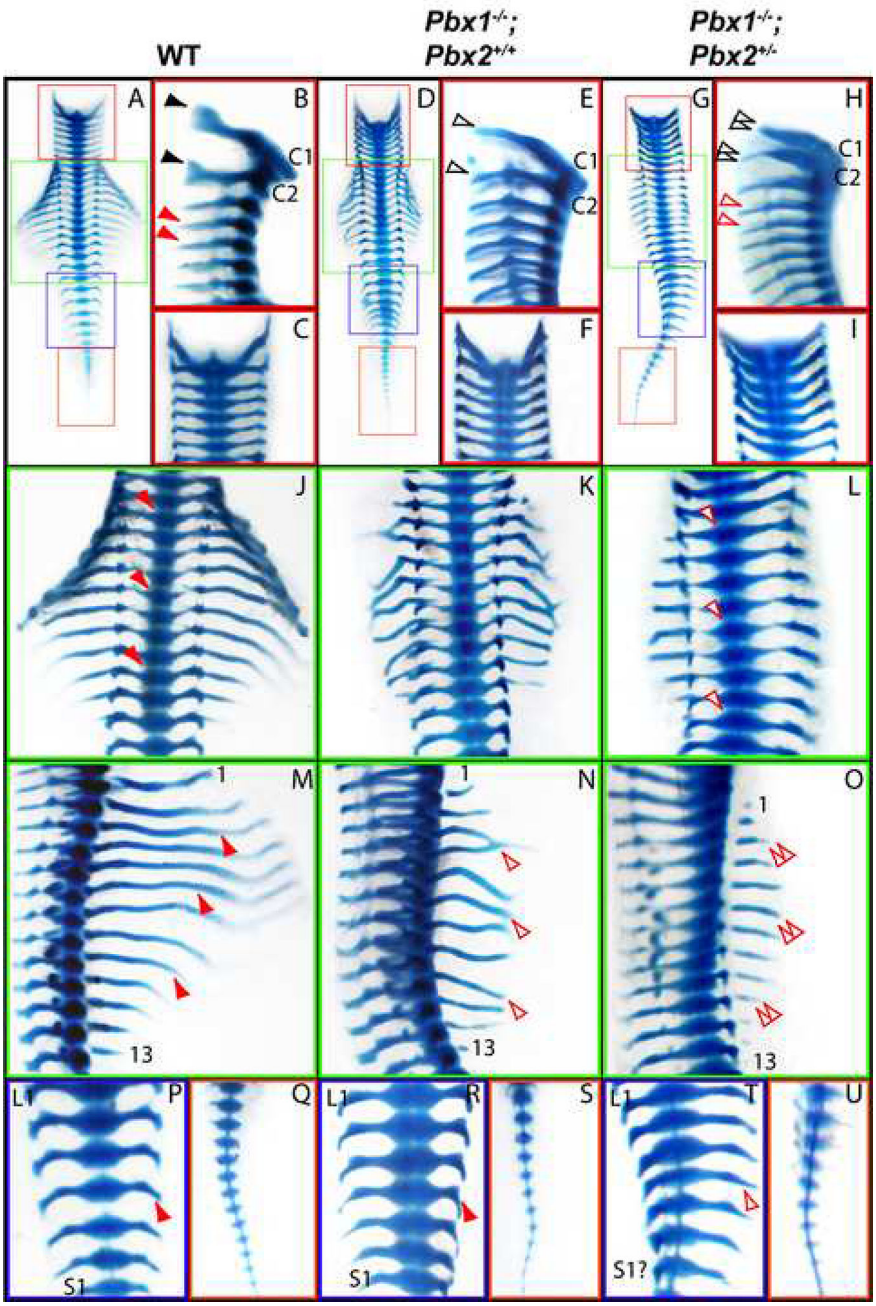

Figure 2. Vertebral and rib skeletal malformations in *Pbx1*$^{-/-}$;*Pbx2*$^{+/+}$ and *Pbx1*$^{-/-}$;*Pbx2*$^{+/-}$ embryos at E13.5

(A,D,G) When compared to WT (A), Alcian Blue staining of E13.5 littermates reveals post-cranial axial defects in *Pbx1*$^{-/-}$;*Pbx2*$^{+/+}$ (D) and *Pbx1*$^{-/-}$;*Pbx2*$^{+/-}$ (G) embryos, as demonstrated in the different colored insets depicting higher magnification views of each vertebral segment. In the cervical region (red insets), when compared to WT (B, C; black and red arrowheads), *Pbx1*$^{-/-}$;*Pbx2*$^{+/+}$ (E, F) and *Pbx1*$^{-/-}$;*Pbx2*$^{+/-}$ embryos (H, I) both display thinning/reduction in the transverse processes of cervical #1 (C1) and C2 (empty black arrowheads), which is more severe in *Pbx1*$^{-/-}$;*Pbx2*$^{+/-}$ embryos (H; double empty black arrowheads). Additionally, the latter display marked reductions in the transverse

processes of lower cervical vertebrae (H, empty red arrowheads). In the thoracic region (J–L), when compared to WT (J; red arrowheads) and *Pbx1*$^{-/-}$;*Pbx2*$^{+/+}$ embryos (K), the vertebral centra of the *Pbx1*$^{-/-}$;*Pbx2*$^{+/-}$ mutants (L) are rostral-caudally flattened and medial-laterally thinned (empty red arrowheads). Also, in the thoracic region (M–O), as compared to WT (M, red arrowheads), *Pbx1*$^{-/-}$;*Pbx2*$^{+/+}$ embryos (N) display distally shortened and markedly dysmorphic ribs (empty red arrowheads), which are often fused, while *Pbx1*$^{-/-}$;*Pbx2*$^{+/-}$ embryos (O) exhibit more severe rib defects with drastically shortened and/or rudimentary elements (double empty red arrowheads). In the lumbar (L1) - sacral (S1) region (P, R, T), the transverse processes of *Pbx1*$^{-/-}$;*Pbx2*$^{+/-}$ embryos (T) are more attenuated and flattened (empty red arrowhead) than seen in both WT (P) and single *Pbx1* mutant embryos (R) (red arrowheads). Finally, no major defects were observed in the caudal vertebral domain (Q, S, U) of these embryos, although the development of their posterior-most domains may be delayed and/or stunted. Rostral (top).

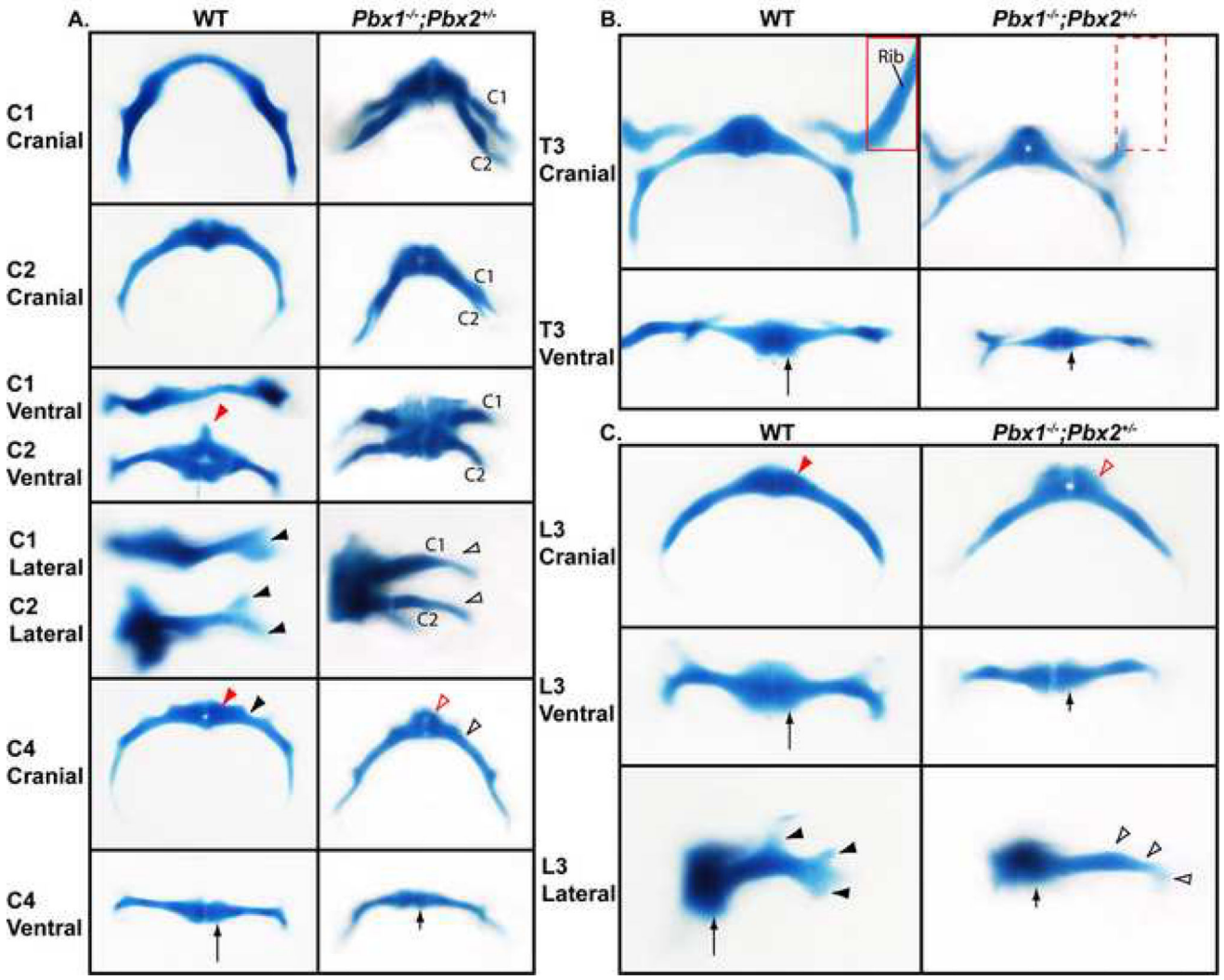

Figure 3. Morphological abnormalities in dissected vertebral elements from *Pbx1*$^{-/-}$;*Pbx2*$^{+/-}$ embryos

Alcian Blue staining of developing vertebrae spanning several axial regions reveals that all vertebral types lose specific features of their axial level identity. (A) Compared to WT (left), in *Pbx1*$^{-/-}$;*Pbx2*$^{+/-}$ embryos (right), C1 and C2 are grossly mis-shapened and fused together as evident from the cranial, ventral, and lateral views. Because of this fusion, no distinct dens (odontoid process) is detectable in *Pbx1*$^{-/-}$;*Pbx2*$^{+/-}$ embryos (right) compared to WT (left, red arrowhead). As evident in the cranial view, the transverse processes in *Pbx1*$^{-/-}$;*Pbx2*$^{+/-}$ C1 and C2 vertebrae (right) project from the body at more acute angles when compared to WT (left). In addition, these mutant transverse processes are thinned (lateral view, empty black arrowheads) and lose specific morphologies that define C1 and C2 identity, compared to WT (lateral view, black arrowheads). The morphology of mutant C4 is also drastically altered compared to WT. In the cranial view, its centrum is more rounded (empty red arrowhead) when compared to the WT (red arrowhead), and the groove for the vertebral artery is absent (empty black arrowhead) compared to WT (black arrowhead). In the ventral view the entire rostral-caudal height of the body is also reduced (short arrow)

compared to WT (long arrow). (B) Compared to WT, all of the developing thoracic vertebrae (represented here by T3) are smaller, the transverse processes project from the body at more acute angles when compared to WT, and the ribs are either rudimentary elements or completely absent (dashed red rectangle) compared to WT (red rectangle) seen in the cranial view. Also, there is a marked reduction in the height of the mutant centra (short arrow) compared to WT (long arrow). (C) Compared to WT centra (red arrowhead and long arrow respectively), the mutant centra of all developing lumbar vertebrae (represented here by L3) are more rounded and flattened (cranial view, empty red arrowhead) and thinner in their overall height (ventral view, short arrow). In the lateral view, this height reduction is evident (short arrow) compared to WT (long arrow), as is the loss of anterior and posterior tubercles (empty black arrowheads) emerging from the transverse process, specifically compared to WT (black arrowheads). In cranial views, ventral views, and lateral views, ventral, rostral, and rostral are towards the top, respectively.

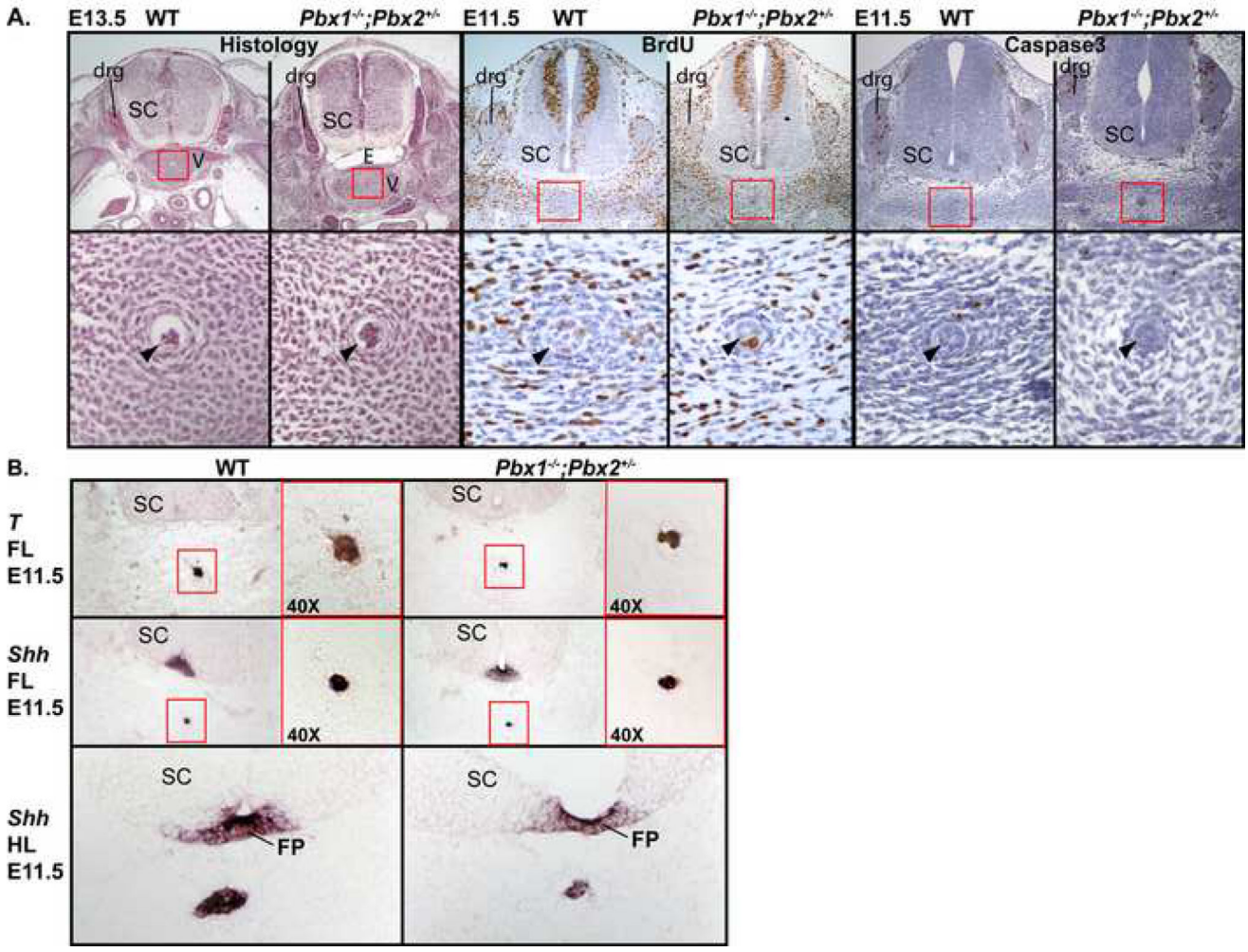

Figure 4. Unperturbed cellular proliferation and programmed cell death in *Pbx1*$^{-/-}$;*Pbx2*$^{+/-}$ notochord and vertebral anlage; unperturbed expression of notochord markers in *Pbx1*$^{-/-}$;*Pbx2*$^{+/-}$ embryos

(A) Unless otherwise noted, all images are transverse sections at the mid-thoracic level and are shown in 10× (upper) panels and 40× (lower) insets. Hematoxylin and Eosin staining of E13.5 transverse sections of *Pbx1*$^{-/-}$;*Pbx2*$^{+/-}$ and WT embryos (left) does not reveal significant differences in the structure and cellular morphology of the notochord but does reveal that the cellular density of vertebral anlagen is reduced compared to WT embryos (black arrowheads depict the notochord). At E13.5, edema is evident between the spinal cord and the vertebral anlagen of *Pbx1*$^{-/-}$;*Pbx2*$^{+/-}$ embryos. Next, at E11.5, cell proliferation as measured by BrdU incorporation is not different in *Pbx1*$^{-/-}$;*Pbx2*$^{+/-}$ notochord and vertebral anlage compared to that present in WT (middle, black arrowheads, insets). Finally, at E11.5, levels of cellular apoptosis, as assayed by Caspase3 antibody staining, do not differ between *Pbx1*$^{-/-}$;*Pbx2*$^{+/-}$ and WT notochord and vertebral anlage (right, black arrowheads, insets). In contrast, higher levels of cellular apoptosis are equally present in *Pbx1*$^{-/-}$;*Pbx2*$^{+/-}$ and WT dorsal root ganglia at these gestational days. (B) *In situ* hybridization on E11.5 transverse sections reveals that the expression of *Brachyury* (*T*) remains unaltered in *Pbx1*$^{-/-}$;*Pbx2*$^{+/-}$ notochord (red inset in 20× (left) and 40× (right) panels) as shown at the

level of the forelimb (FL). Similarly, at E11.5, *Shh* expression remains unaltered in the notochord and neural floor plate in *Pbx1*$^{-/-}$;*Pbx2*$^{+/-}$ mutants as shown at both forelimb (FL) and hindlimb (HL) axial levels. Drg, dorsal root ganglion; E, edema; FP, Floor Plate; SC, spinal cord; V, vertebra. Dorsal (top).

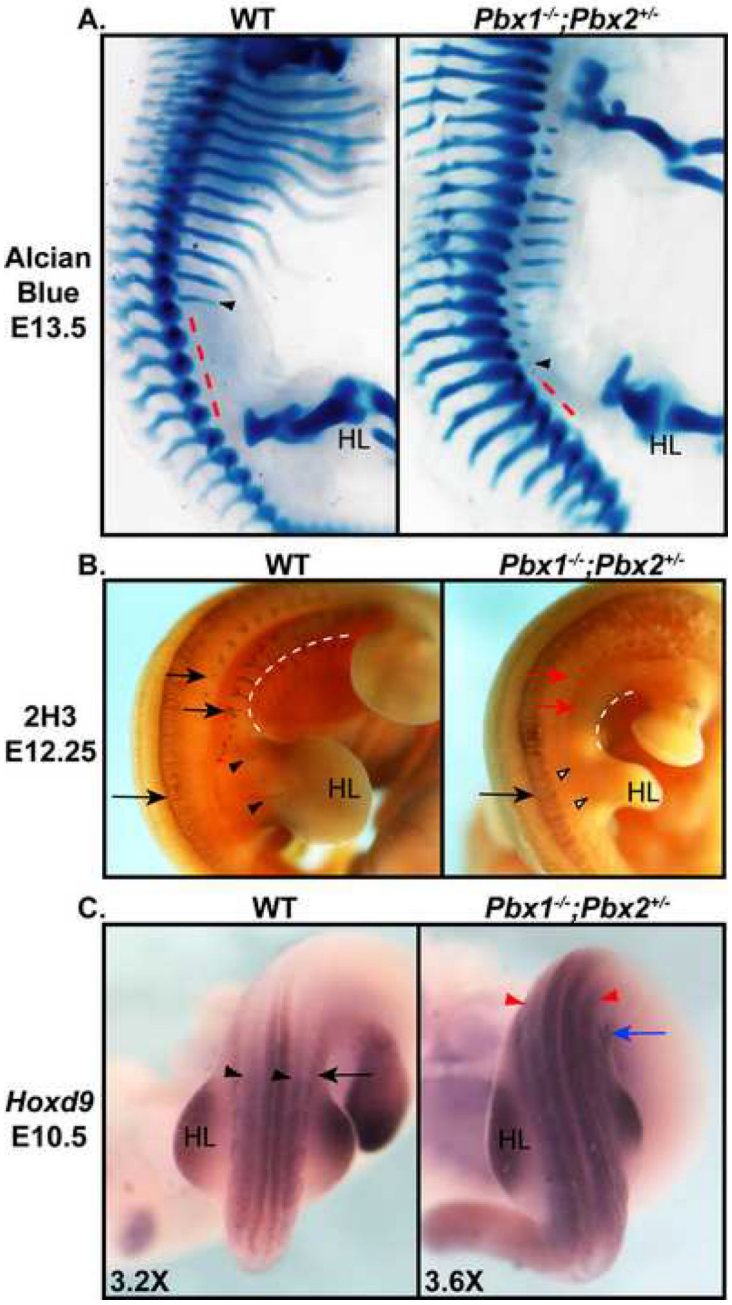

Figure 5. Hindlimb bud position is shifted in *Pbx1*$^{-/-}$;*Pbx2*$^{+/-}$ embryos and is associated with alterations in posterior neurogenesis and *Hox* expression

(A) Alcian Blue staining of E13.5 *Pbx1*$^{-/-}$;*Pbx2*$^{+/-}$ and WT littermates reveals that with respect to the most caudal rib-bearing thoracic vertebra (black arrowheads), the mutant pelvic girdle (and hindlimb) is shifted rostrally by at least two vertebrae (dashed red-lines). (B) Earlier at E12.25, 2H3 antibody staining for neurofilament localization demonstrates that in *Pbx1*$^{-/-}$;*Pbx2*$^{+/-}$ embryos hindlimb bud position is also rostrally shifted and, while forelimb bud position remains relatively stable, the distance (described by the white dashed lines) spanning both limb types is markedly reduced compared to WT. Neurofilament staining also demonstrates that despite similar staining in the neuroectoderm (long black

arrows in mutant and WT), in the mutant neurogenesis becomes severely compromised more caudally along the embryo, specifically in the lateral and ventral extent of projecting neural fibers (short red arrows) when compared to WT patterns (short black arrows). Furthermore, the neuronal fibers that normally enter the hindlimb field, as seen in WT (black arrowheads), are not present in the mutant (empty black arrowheads) at this day. (C) *In situ* hybridization at E10.5 reveals that *Hoxd9* expression is rostralized and up-regulated in the somites (red arrowheads) and LPM (blue arrow) in $Pbx1^{-/-};Pbx2^{+/-}$ embryos when compared to WT (black arrowheads and arrow, respectively). HL, hindlimb. Rostral (top)

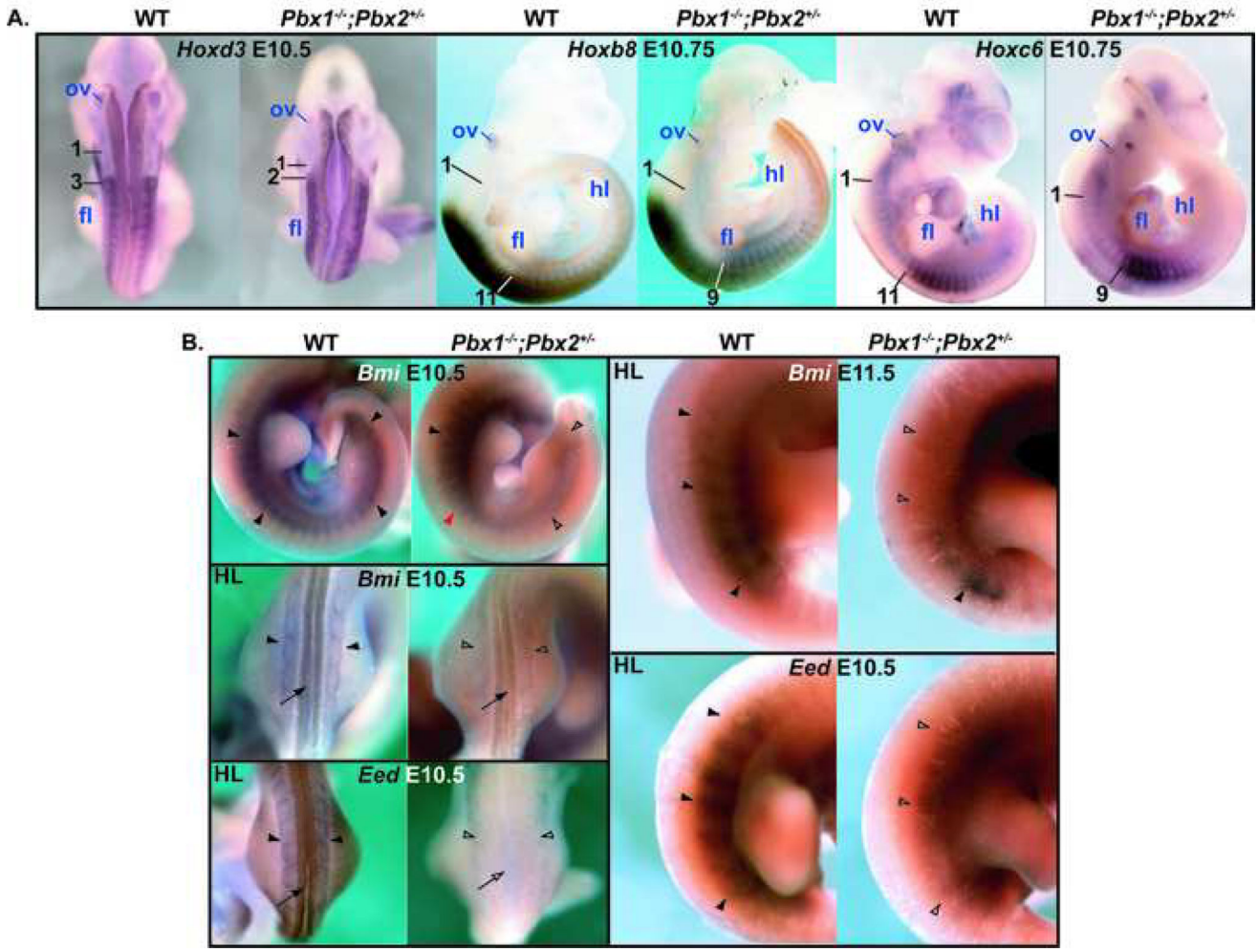

Figure 6. Alterations in axial vertebral morphological identity and hindlimb bud position in *Pbx1*$^{-/-}$;*Pbx2*$^{+/-}$ embryos are associated with rostral shifts in the expression of *Hox* and down-regulations of Polycomb group genes, *Bmi/Eed*, along the embryonic axis

(A) When compared to WT, at E10.5–10.75, the rostral extent of expression of *Hoxd3, Hoxb8*, and *Hoxc6* is shifted rostrally by approximately 1–3 somites in *Pbx1*$^{-/-}$;*Pbx2*$^{+/-}$ embryos (compare somite numbers in WT and mutant) specifically with respect to the first somite (denoted by somite #1). Note: the *Pbx1*$^{-/-}$;*Pbx2*$^{+/-}$ embryos shown for *Hoxb8* and *Hoxc6* display a slight anteriorization of the forelimb bud position. (B) When compared to WT (black arrowheads in all panels), in *Pbx1*$^{-/-}$;*Pbx2*$^{+/-}$ embryos, the expression of *Bmi* is severely reduced at E10.5 along the entire posterior embryo (top; red arrowhead and empty black arrowheads) and specifically reduced, if not absent, in the somites adjacent to the hindlimb buds at E10.5 (below; empty black arrowheads) and at E11.5 (right; empty black arrowheads), though it remains expressed in the neuroectoderm (E10.5, below; black arrow). At these same gestational days, when compared to WT (black arrowheads), *Eed* expression (below and right) is also severely reduced posteriorly in the mutant (empty black arrowheads), and even from the neuroectoderm (E10.5, below; empty black arrow). FL, forelimb; HL, hindlimb; ov, otic vesicle. Rostral (top).

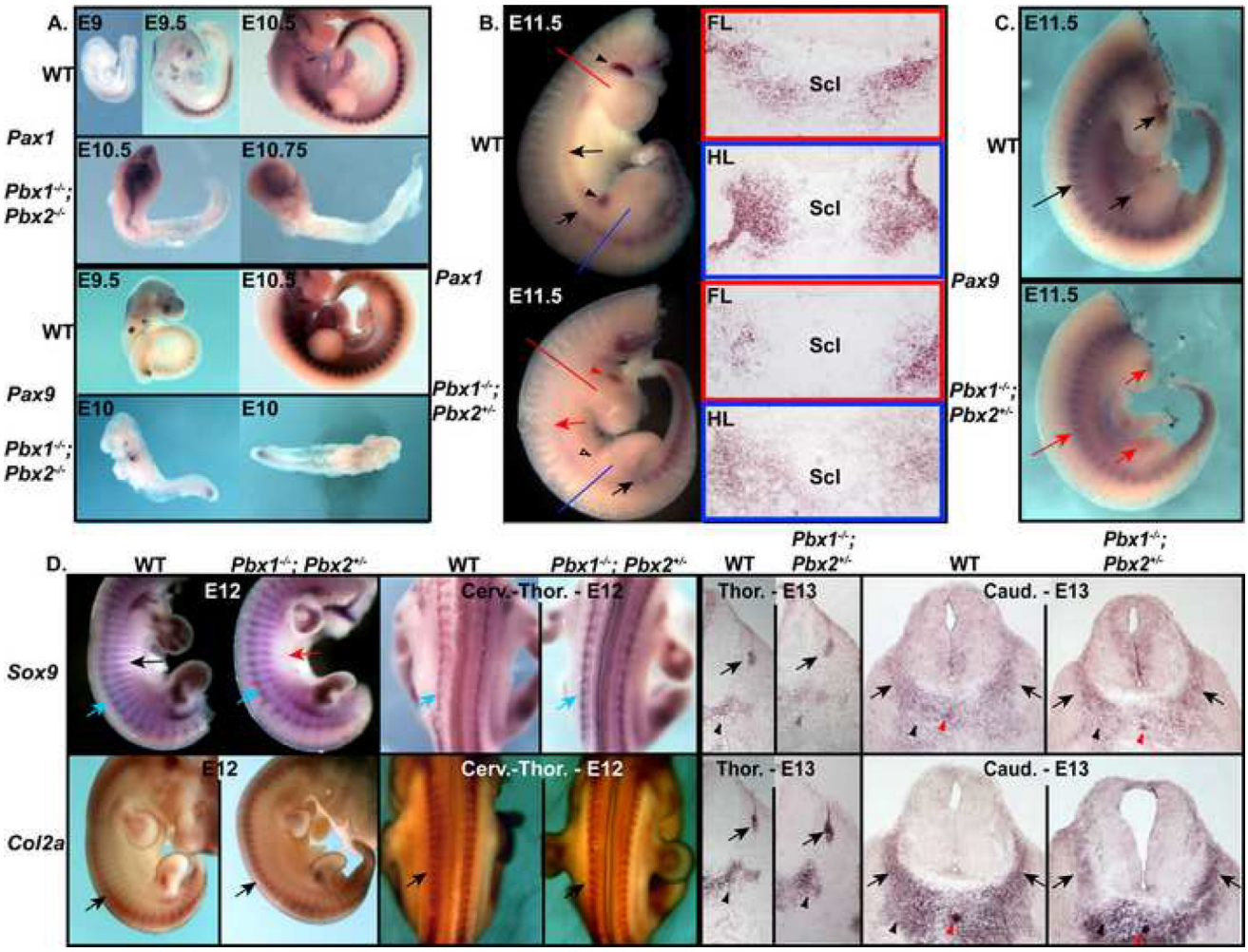

Figure 7. Alterations in vertebral morphogenesis are associated with down-regulations of *Pax1* and *Pax9* somitic mesodermal and sclerotomal expression in *Pbx1*$^{-/-}$;*Pbx2*$^{-/-}$ and *Pbx1*$^{-/-}$;*Pbx2*$^{+/-}$ embryos but not with changes in marker gene expression for mesenchymal and cartilage cell differentiation

(A) *In situ* hybridization of *Pax1* (top) and *Pax9* (bottom) on WT and *Pbx1*$^{-/-}$;*Pbx2*$^{-/-}$ embryos spanning gestational days E9–E10.75 demonstrates that the expression of both genes is absent from the developing somites of double knockout embryos. *Pax1* expression is completely absent from the developing somites of double mutant embryos (2 embryos shown) unlike the WT expression pattern at several different gestational days. The signal present in the cranial region represents background trapping of the probe. Similarly, when compared to WT embryos at different gestational days, *Pax9* is absent in the somites of double mutant embryos (2 embryos shown), yet low levels of expression are detected most caudally in their pre-somitic mesoderm. (B) *In situ* hybridization of *Pax1* on WT and *Pbx1*$^{-/-}$;*Pbx2*$^{+/-}$ embryos at E11.5 demonstrates that it is down-regulated in the sclerotome of the compound mutant. Specifically, on whole embryos (left), *Pax1* expression is markedly reduced posteriorly in the mutant as its expression is reduced along the flank (red arrow) and forelimb (red arrowhead), absent from the proximal hindlimb bud (empty black arrowhead), and spatially restricted to caudal somites (black arrow) compared to the levels seen in WT embryos (black arrows and arrowheads, respectively). Additionally, section *in situ*

hybridization at the axial levels of the forelimb (FL, red inset on right) and hindlimb (HL, blue inset on right) demonstrates that *Pax1* is spatially diffused in the sclerotome (Scl) in *Pbx1*$^{-/-}$;*Pbx2*$^{+/-}$ embryos. (C) *Pax9* expression on whole mount E11.5 mutant embryos is reduced along the entire axis but not to the same extent as seen for *Pax1*; specifically, it is reduced in the anterior forelimb and hindlimb buds (short red arrows) and is down-regulated in the differentiating somites (long red arrow) of the mutant compared to the WT (black long and short arrows, respectively). (D) *Sox9* and *Col2a1*, markers of mesenchymal condensation and cartilage cell differentiation, respectively, remain relatively unchanged between WT and *Pbx1*$^{-/-}$;*Pbx2*$^{+/-}$ embryos as revealed by whole-mount (left) and section (right) *in situ* hybridization. By whole-mount, *Sox9* (blue arrows) and *Col2a1* (black arrows) are well-expressed in WT and *Pbx1*$^{-/-}$;*Pbx2*$^{+/-}$ vertebral bodies at E12 as shown in lateral and dorsal views, although *Sox9* is absent in areas where ribs should form in *Pbx1*$^{-/-}$;*Pbx2*$^{+/-}$ embryos (red arrow) compared to WT (black arrow). By section at E13 (right, top), *Sox9* is slightly reduced in the thoracic vertebral body mesenchyme of *Pbx1*$^{-/-}$;*Pbx2*$^{+/-}$ embryos (gray arrowhead) compared to WT (black arrowhead), while strong and normal signals are detected for this gene in both thoracic and caudal neural arches (black arrows), and caudal body mesenchyme (black arrowheads) and notochords (red arrowheads). Also at E13, *Col2a1* expression (right, bottom) remains unaltered in developing thoracic and caudal vertebral structures in *Pbx1*$^{-/-}$;*Pbx2*$^{+/-}$ embryos compared to WT embryos, even in those embryos where neural tube defects are evident. Scl, sclerotome. In (A) WT Rostral (top), *Pbx1*$^{-/-}$;*Pbx2*$^{-/-}$ (left); In (B–C) Rostral (top); In (D, whole-mounts) Rostral (top); In (D, sections) Dorsal (top).

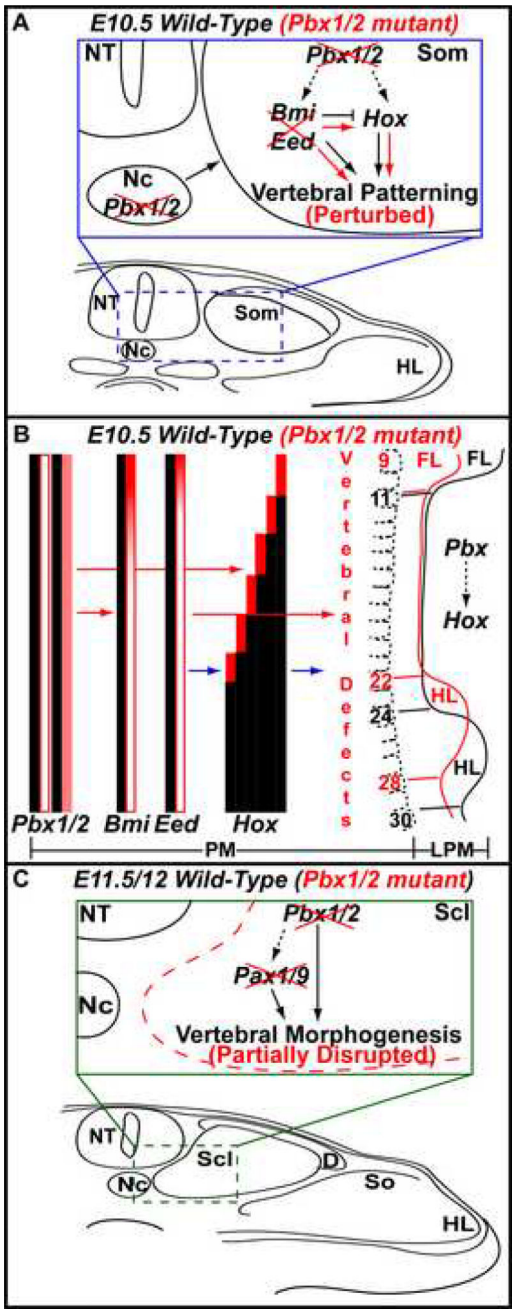

Figure 8. Proposed model of Pbx1/Pbx2 function during vertebral patterning and morphogenesis

(A–C) In all panels, black arrows, inhibitory lines, text, bars, and diagrammatic sketches represent wildtype conditions and the proposed genetic roles of Pbx, while all corresponding red signatures reflect events or processes that occur in the *Pbx1*$^{-/-}$;*Pbx2*$^{+/-}$ (*Pbx1/2 mutant*) embryo. (A) Proposed genetic roles of *Pbx1/Pbx2* during vertebral patterning. As represented in a transverse section at the early hindlimb bud (HL) axial level at E10.5 (blue inset), *Pbx1/Pbx2* are normally expressed in the notochord (Nc) and developing somite (Som). The loss of *Pbx* from the Nc (red cross), as occurs in the *Pbx1/2 mutant*, does not alter signaling to the ventro-medial somite, as indicated by the black arrow. Conversely, the

loss of *Pbx1/Pbx2* from the somite causes perturbed vertebral patterning via their primary genetic control on the expression of Polycomb group genes (i.e., *Bmi/Eed*) and concomitant secondary control of *Hox* genes, although this latter relationship may also be indirect via a loss of Polycomb repression on *Hox* transcription (see (B) and text for more details). (B, left) The proposed genetic relationships between *Pbx1/Pbx2, Bmi/Eed, Hox*, and vertebral patterning in the paraxial mesoderm (PM) are also summarized in a cranial-caudal depiction of a developing embryonic axis at E10.5. According to the wildtype pattern (black bars overlying each gene name), *Pbx1/Pbx2* and *Bmi/Eed* are normally expressed along the entire axis of the embryo, while *Hox* genes are expressed in nested and graded domains spanning cranial to caudal somites (only mid-thoracic to sacral somites are shown on the right). In the absence of *Pbx1* (empty red bar) and partial absence of *Pbx2* (shaded pink bar due to its heterozygous state in the *Pbx1/2 mutant*), *Bmi/Eed* expression is reduced (short red arrow) along the axis, most notably posteriorly (graded red to white bars), which may primarily lead to the vertebral patterning defects along the entire axis (red arrow). Concomitantly, loss of repression of *Hox* gene transcription and rostralization of *Hox* signal (red bars above black bars, spanning higher somite numbers, shown to the right) may also in part contribute to the etiology of these defects. In this diagram, the solid blue arrow indicates previously published relationships, whereas the solid red arrows depict roles revealed in this paper. (B, right) The changes identified in the PM are coincident with, but not necessarily causative of, the alterations in limb bud positions as occurring in the LPM. Specifically, in the absence of *Pbx1/Pbx2* (red line diagram) and their control on *Hox*, HL are rostrally shifted by 2 or more somites compared to the wildtype pattern (black line diagram). (C) Proposed genetic roles of *Pbx* during sclerotomal formation and vertebral morphogenesis. As represented in the green inset of a transverse section at the HL bud axial level at E11.5/12, *Pbx1/Pbx2* are normally expressed in the developing sclerotome (Scl) where they are upstream genetically of *Pax1/Pax9*. The loss of *Pbx1/Pbx2* from this tissue (red cross) influences vertebral morphogenesis via perturbations of the expression of *Pax1/Pax9*, critical markers of the sclerotome (red cross). See text for details. D, dermomyotome; FL, forelimb; HL, hindlimb; LPM, lateral plate mesoderm; Nc, notochord; NT, neural tube; PM, paraxial mesoderm; Scl, sclerotome; So, somatopleure; Som, somite. In (A and C), Ventral (bottom) and Lateral (right); in (B), Rostral (top).

Table 1

Gene	Genotype[1]	Gest. Day[2]	FL range[3]	HL range[4]	Signal Start[3]
Hoxd3	WT	E10.5	7 to 11	24 to 29	3
	Pbx1$^{-/-}$;*Pbx2*$^{+/-}$	E10.5	7 to 11	22 to 27	1 to 2
Hoxb8	WT	E10.75	7 to 11	24 to 29	11
	Pbx1$^{-/-}$;*Pbx2*$^{+/-}$	E10.75	7 to 11	23 to 28	9
Hoxc6	WT	E10.75	7 to 11	24 to 29	11
	Pbx1$^{-/-}$;*Pbx2*$^{+/-}$	E10.75	6/7 to 11	22 to 27	9

[1] 3 mutant/WT pairs were observed for each day

[2] All embryos were somite-matched

[3] Values refer to the rostral-most level in somite position(s) in each embryo

[4] Values refer to the caudal-most level in somite position(s) in each embryo